Delineating antibody responses elicited by four SARS-CoV-2 variants against the Mu variant

Student Name: Prudence Kgagudi

Student Number: 2579428

MASTER OF SCIENCE IN MEDICINE (MRA05)

RESEARCH THESIS

08 June 2023

Supervisors:

Dr Thandeka Moyo-Gwete, PhD

Co-supervisor: Dr Simone I. Richardson, PhD

Co-Supervisor: Prof. Penny L. Moore, PhD

Table of Contents

List of Figures

List of Tables

UNIVERSITY OF THE WITWATERSRAND, JOHANNESBURG

FACULTY OF HEALTH SCIENCES

Declaration

I, Prudence Kgagudi (Student number: 2579428) am a student registered for MSc (MED) in the academic year 2023. I hereby declare the following:

I am aware that plagiarism (the use of someone else's work without their permission and/or without acknowledging the original source) is wrong.

I confirm that the work submitted for assessment for the above degree is my own unaided work except where I have explicitly indicated otherwise.

I have followed the required conventions in referencing the thoughts and ideas of others.

I understand that the University of the Witwatersrand may take disciplinary action against me if there is a belief that this is not my own unaided work or that I have failed to acknowledge the source of the ideas or words in my writing.

I have included as an appendix a report from "Turnitin" (or other approved plagiarism detection) software indicating the level of plagiarism in my research document.

Prudence Kgagudi

Date: 08th June 2023

Presentations

Kgagudi, P., Manamela, N., Makhado, N., Ayres, F., Mhlongo, D., Van der Mescht, M., De Beer, Z., De Villiers, T. R., Burgers, W. A., Ntusi, N., Rossouw, T., Ueckermann, V., Boswell, M. T., Richardson, S. I., Moore, P. L., Moyo-Gwete, T. (2022) 'Mu variant shows variable escape from humoral responses triggered by four different variants', 11th Infectious Diseases in Africa Symposium. 2022. Oral presentation and poster.

Publications

Richardson, S. I., Kgagudi, P., Manamela, N. P., Kaldine, H., Venter, E. M., Pillay, T., Lambson, B. E., Van Der Mescht, M. A., Hermanus, T., De Beer, Z., Roma De Villiers, T., Bodenstein, A., Van Den Berg, G., Du Pisanie, M., Burgers, W. A., Ntusi, N. A. B., Ueckermann, V., Rossouw, T. M., Boswell, M. T., & Moore, P. L. (n.d.). *Fc effector activity and neutralization against SARS-CoV-2 BA.4 is compromised in convalescent sera, regardless of the infecting variant*. https://doi.org/10.1101/2022.07.14.500042

Moyo-Gwete, T., Madzivhandila, M., Mkhize, N. N., Kgagudi, P., Ayres, F., Lambson, B. E., Manamela, N. P., Richardson, S. I., Makhado, Z., Mescht, M. A. van der, Beer, Z. de, Villiers, T. R. de, Burgers, W. A., Ntusi, N. A. B., Rossouw, T., Ueckermann, V., Boswell, M. T., & Moore, P. L. (2022). Shared N417-Dependent Epitope on the SARS-CoV-2 Omicron, Beta, and Delta Plus Variants. *Journal of Virology*. https://doi.org/10.1128/JVI.00558-22

Moyo-Gwete, T., Madzivhandila, M., Makhado, Z., Ayres, F., Mhlanga, D., Oosthuysen, B., Lambson, B. E., Kgagudi, P., Tegally, H., Iranzadeh, A., Doolabh, D., Tyers, L., Chinhoyi, L. R., Mennen, M., Skelem, S., Marais, G., Wibmer, C. K., Bhiman, J. N., Ueckermann, V., … Moore, P. L. (2021). Cross-Reactive Neutralizing Antibody Responses Elicited by SARS-CoV-2 501Y.V2 (B.1.351). *New England Journal of Medicine*, *384*(22), 2161–2163. https://doi.org/10.1056/nejmc2104192

Wibmer, C. K., Ayres, F., Hermanus, T., Madzivhandila, M., Kgagudi, P., Oosthuysen, B., Lambson, B. E., Oliveira, T. de, Vermeulen, M., Berg, K. van der, Rossouw, T., Boswell, M., Ueckermann, V., Meiring, S., Gottberg, A. von, Cohen, C., Morris, L., Bhiman, J. N., & Moore, P. L. (2021). SARS-CoV-2 501Y.V2 escapes neutralization by South African COVID-19 donor plasma. *Nature Medicine 2021 27:4*, *27*(4), 622–625. https://doi.org/10.1038/s41591-021-01285-x

Scheepers, C., Everatt, J., Amoako, D. G., Tegally, H., Wibmer, C. K., Mnguni, A., Ismail, A., Mahlangu, B., Lambson, B. E., Richardson, S. I., Martin, D. P., Wilkinson, E., San, J. E., Giandhari, J., Manamela, N., Ntuli, N., Kgagudi, P., Cele, S., Pillay, S., … Bhiman, J. N. (2021). Emergence and phenotypic characterization of C.1.2, a globally detected lineage that rapidly accumulated mutations of concern. *MedRxiv*, 2021.08.20.21262342. https://doi.org/10.1101/2021.08.20.21262342

Dedication

I dedicate this work to my husband Isaac and son Botshelo Diale, my greatest cheerleaders and source of strength. Thank you for your love, believing in me and the endless milkshake supply. To Botshelo, thank you for the constant check-ups when I don't leave my laptop, for the coffee supply and Saturday morning breakfasts.

Acknowledgements

To my primary supervisor Dr. Thandeka Moyo-Gwete you are a remarkable supervisor and thank you for the positive energy. Dr Simone Richardson thank you for sharing your expertise and advice. Prof. Penny Moore for giving me this opportunity, additional supervision and for providing funding.

To my sister, brother and niece (Duba Family): Thank you for your support, always willing to step in and help with parenting duties.

Lastly, thank you to all the Antibody Immunity Research Unit staff and students for all the training provided, support and guidance.

Abstract

SARS-CoV-2 is the causative agent of the acute respiratory syndrome known as coronavirus disease 2019 (COVID-19). The SARS-CoV-2 spike protein plays an essential role in virus attachment, fusion and entry and is the main target of neutralizing antibodies. Continued evolution of the spike has led to the emergence of variants of concern or interest (VOC/VOIs) which pose a greater risk to the population due to augmented transmission risk, increased disease severity, antigenic escape and/or decreased effectiveness of vaccines. The Mu variant was first identified in Columbia in January 2021, however the immune escape potential of the variant remains poorly characterised. It is typified by T95I, Y144S and Y145N mutations in the N-terminal domain; R346K, E484K, and N501Y mutations in the receptor-binding domain and D614G, P681H, and D950N mutations in the S2 region. This study aimed to assess targeting of the Mu variant by neutralizing and non-neutralizing antibodies elicited by four variants during four COVID-19 waves in South Africa namely D614G, Beta, Delta and Omicron (BA.1). This was achieved by measuring antibody binding, neutralization and antibody dependent cellular cytotoxicity (ADCC) activity against Mu, and comparing these responses across each of the four variants tested. All variants elicited cross-reactive binding antibodies to Mu although the magnitude of binding to Mu was reduced. This cross-reactivity was a result of multiple binding antibody epitopes on the spike protein. We observed variable neutralization escape of Mu from antibodies triggered by infection with WT D614G and Delta. Antibodies induced by the Beta variant exhibited increased breadth towards the Mu variant when compared to those elicited by other variants. Neutralization escape of Mu from antibodies elicited by WT D614G and Delta may be caused by the 95I, 484K and 346K mutations in Mu, which are known to confer resistance in other variants. Compared to neutralization, ADCC was mostly preserved against Mu. However, the infecting variant impacted the potency of ADCC responses. WT D614G triggered significantly higher ADCC activity against Mu compared to Beta, Delta and Omicron. These data suggest that different variants trigger qualitatively different neutralizing and Fc effector responses, providing a rationale to study humoral resistance following infection by different variants. As Mu shares mutations with other VOCs, this study may aid in predicting the impact of mutations that may be common to emerging VOCs.

Abbreviations

ACE2	Angiotensin Converting Enzyme 2
ADCC	Antibody Dependent Cellular Cytotoxicity
COVID-19	Coronavirus Disease 2019
DMEM	Dulbecco’s Modified Eagle’s Medium
DNA	Deoxyribonucleic acid
ELISA	Enzyme linked immunosorbent assay
FBS	Fetal bovine serum
Fc	Fragment crystallisable
HC	Heavy chain
HEK	Human Kidney Embryonic
HR1	Heptad repeat 1
HR2	Heptad repeat 2
ID50	Inhibitory Dilution (at 50% inhibition)
IDMD	Iscove's Modified Dulbecco's Medium
IgM	ImmunoglobulinM
kDa	Kilo Dalton
LC	Light chain
LB	Lauria Bertoni
mAb	Monoclonal antibody

nAbs	Neutralizing antibodies
Nsps	Non-structural proteins
NTD	N-terminal domain
Opti-MEM	Optimal minimal essential media
PBS	Phosphate Buffered Saline
PCR	Polymerase chain reaction
PEI-MAX	Polyethylenimine hydrochloride max
RBD	Receptor binding domain
RLU	Relative light units
RPM	Revolutions per minute
SARS-CoV-2	Severe Acute Respiratory Syndrome Coronavirus 2
SDS-PAGE	Sodium dodecyl sulphate polyacrylamide gel electrophoresis
SEC	Size exclusion chromatography
TM	Transmembrane domain
TMB	3,3'5,5'-Tetramethylbenzidine
VOC	Variant of Concern
VOI	Variant of Interest
WT	Wild type

1. Introduction

1.1 The SARS-CoV-2 pandemic

Severe Acute Respiratory Syndrome Coronavirus 2 (SARS-CoV-2) is the causative agent of coronavirus disease 2019 (COVID-19) (Gorbalenya, Baker, Baric, Groot, *et al.*, 2020). It caused a global pandemic since it was initially detected in Wuhan, China late in 2019. SARS-CoV-2 is of zoonotic origin and shares genomic similarity with other zoonotic coronaviruses including SARS-CoV-1 and Middle East Respiratory Syndrome Coronavirus (Ye *et al.*, 2020).

There were over 675 million reported COVID-19 cases and 6.87 million COVID-19 related deaths globally. South Africa, accounted for over 4 million cases and 102 595 deaths (WHO, 2023). South Africa's first wave was driven by WT D614G, the second wave by Beta, third wave by Delta, fourth wave by BA.1 while the fifth wave was driven by BA.4 **(Figure 1.1)**.

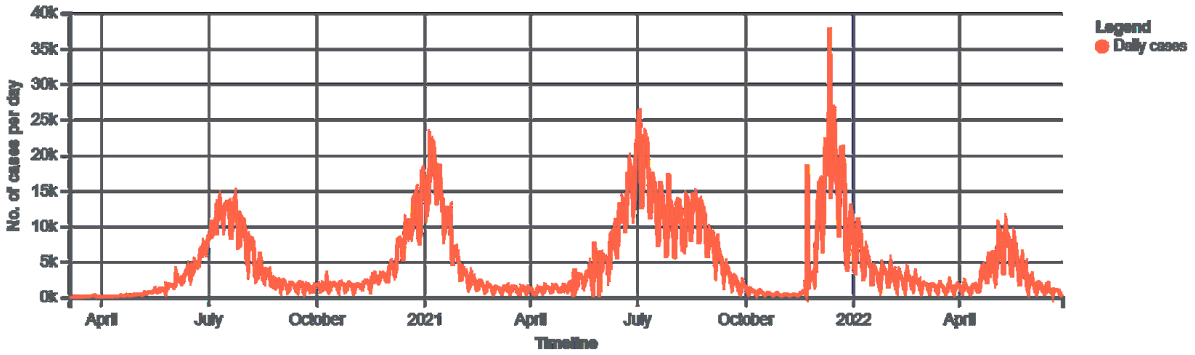

Figure 1. 1 Waves of SARS-CoV-2 infections in South Africa. The graph shows the number of new cases per day in South Africa from the 5th of March 2020 to April 2022 (WHO, 2023)

The rapid spread of the virus highlighted the urgent need to find preventative and curative strategies which include vaccines and therapeutic interventions such as monoclonal antibodies (mAbs) and convalescent plasma. Early in the pandemic, convalescent plasma was considered as a favourable COVID-19 therapy and received authorization for emergency use by the U.S. Food and Drug Administration however studies show it was not effective (Zhao and He, 2020; Brobst and Borger, 2022; Elsaghir and Adnan, 2022). Several mAbs were also tested for their capacity to avert or cure SARS–CoV-2 infection in animal models with differing results (Hansen *et al.*, 2020; Rogers *et al.*, 2020). Ultimately the goal is to search for an effective

prophylactic that can prevent infection or generate protective immunity that is durable and SARS–CoV-2 vaccines are likely to be the best solution.

COVID-19 vaccines have shown up to 85% efficacy (Polack et al., 2020) in preventing infection and up to 96% efficacy in preventing severe disease or admission to hospital in settings with the WT D614G variant (Baden et al., 2020; Alter et al., 2021). However, the emergence of variants of interest or concern which reduced vaccine efficacy against symptomatic infection highlighted the importance of viral genomic surveillance, studying immune escape from convalescent sera and analysis of breakthrough infection in vaccinated individuals.

1.2 SARS-CoV-2 Structure

SARS-CoV-2 is an enveloped, positive sense single stranded RNA virus, from the genus *Betacoronaviruses* within the *coronaviridae* family (Gorbalenya *et al.*, 2020). The genetic makeup of SARS-CoV-2 consists of roughly 29 903 nucleotides encoding 9860 amino acids (Rastogi *et al.*, 2020) **(Figure 1.2)**. The viral genome bound to nucleocapsid consists of 5′ and 3′ untranslated regions (UTRs) are critical for gene expression and modulation. The viral membrane is covered with the structural spike glycoprotein, envelope (E), and membrane (M) proteins (Cevik *et al.*, 2020) **(Figure 1.2 &1.3B)**. The M protein is enclosed in the membrane and shapes the virion envelope and the E protein is crucial for coronavirus infectivity (Srinivasan *et al.*, 2020).

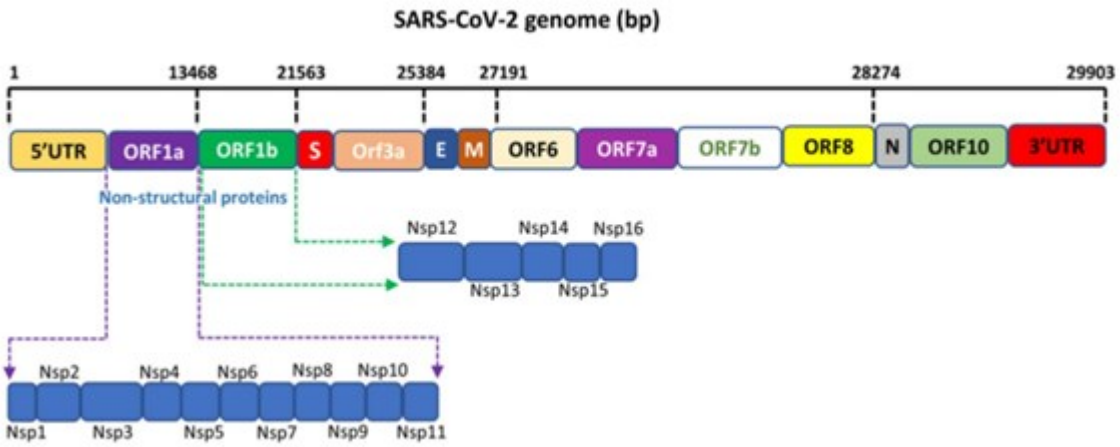

Figure 1. 2 Diagram of the SARS-CoV-2 genome. The genomic organization of the SARS-CoV-2 shows sequential arrangement of various non-structural, structural and accessory genes. The 5′- cap leader and a 3′- polyacetylated tail are bordered by 5′ and 3′ untranslated region (UTRs). The genome

is composed of eight Open reading frames (ORFs) that translate into multiple proteins. Structural proteins, include the spike (S), envelope (E), membrane (M), and nucleocapsid (N) proteins near the 3'end (Gupta *et al.*, 2021)

Open reading frames, ORF1a and1b are responsible for producing 2 polypeptides, pp1a and 1ab. Proteolytic division of pp1a and 1b forms non-structural proteins (Nsps) (Rando *et al.*, 2021). Nsp12 is known as RNA-dependent RNA polymerase and Nsp13 (helicase) generates double membrane vesicles for viral genome replication, transcription, and RNA transport (Gupta *et al.*, 2021).

1.3 SARS-CoV-2 spike glycoprotein

The SARS-CoV-2 Spike glycoprotein is a trimeric class 1 fusion protein. It is responsible for initiating viral entry through the host cellular receptor angiotensin-converting enzyme 2 (ACE-2) (Yan *et al.*, 2020) **(Figure 1.3)**. The spike glycoprotein consists of trimers and contains two operative subunits, one responsible for attachment to the host cell receptor (S1 subunit) and the other for integrating the viral and cellular membranes (S2 subunit) (Walls *et al.*, 2020) **(Figure 1.4B)**. The S1 subunit includes a N-terminal domain (NTD) (14–305 residues) and receptor binding domain (RBD) (319–541 residues). The S2 subunit is made up of the fusion peptide (FP) (788–806 residues), heptapeptide repeat sequence 1 (HR1), HR2 and the TM **(Figure 1.4A)** (Xia *et al.*, 2020).

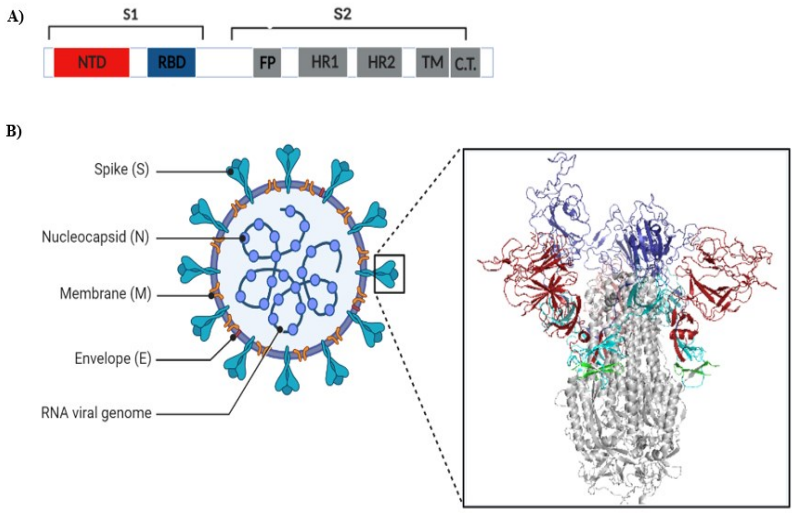

Figure 1. 3 Structure of SARS-CoV-2 spike. (**A**) Schematic of SARS-CoV-2 spike primary structure colored by domain. NTD, N-terminal domain; RBD, receptor-binding domain;The S2 is made up of the fusion peptide (FP),, heptad repeat 1 and 2 (HR1 & 2); 2transmembrane domain (TM),and, cytoplasmic tail (CT). (**B**) SARS-COV-2 virion with a zoomed in spike protein. The SARS-CoV-2 structure was

obtained from the protein databank (PDB ID:7WZ2) and the figure was created using BioRender and Pymol (version 2.3.4).

1.4 Antibody responses to SARS-CoV-2 spike

Antibodies are proteins generated by the adaptive immune system in response to infection (Alberts *et al.*, 2002). Antibodies form a Y-shaped structure made up of two matching light chains (LCs) and two matching heavy chains (HCs) (Chiu *et al.*, 2019) **(Figure 1.4)**. The antigen-binding fragment (Fab) is responsible for antigen binding and neutralizing viruses while the crystallizable fragment (Fc) elicits Fc effector mediated functions against infected cells, such as antibody-dependent cellular cytotoxicity (ADCC), antibody-dependent cellular phagocytosis (ADCP), antibody-dependent complement deposition (ADCD) and antibody-dependent cellular trogocytosis (ADCT) (van Erp *et al.*, 2019; Richardson and Moore, 2021). Both light and heavy chains are further divided into regions referred to as variable (V) and constant (C) regions (Janda *et al.*, 2016). The hinge region confers flexibility of the antibody and is flanked by the CH1 and CH2 domains. Cysteine residues of the HC connect the HC polypeptides by disulphide bonds thus enhancing their antigen-binding potential (Estes *et al.*, 2021) **(Figure 1.4)**.

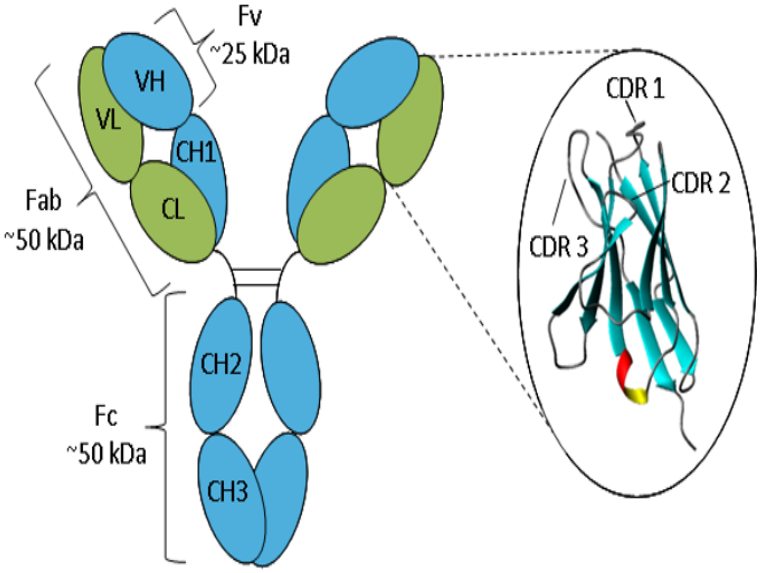

Figure 1. 4 Schematic representation of an antibody. Heavy chains are shown in blue and the light chains are shown in green folded into constant and variable domains. The hinge connects the Fab and Fc. CDR loops are shown on the expansion as ribbons.

Most individuals develop antibodies followingSARS-CoV-2 infection and disease severity correlates with a more robust antibody response (Seow *et al.*, 2020). Immunoglobulin M (IgM) levels peaks at two weeks while IgG levels peak at four weeks after onset of symptoms (Yu *et al.*, 2020), antibody levels remain detectable for at least 16 months (Yang *et al.*, 2022). Mathematical models using sera from humans and non-human primate studies suggest that neutralizing antibodies are a correlate of immune protection against SARS-CoV-2 (Corbett *et al.*, 2020; Khoury *et al.*, 2021; Lim and Cowling, 2022). Mechanisms used by neutralizing antibodies (nAbs) to protect against SARS-CoV-2 infection include hindering interaction between the viral RBD and host ACE- 2 receptor (Xiaojie *et al.*, 2021) or inhibiting membrane fusion (Li *et al.*, 2022; Luo *et al.*, 2022).

1.4.1 SARS-CoV-2 spike neutralizing antibody epitope targets

RBD-specific mAbs have been isolated and classified into categories based on their approach to bind to specific RBD epitopes (Barnes *et al.*, 2020; Jin, Wei and Sun, 2021) **(Figure 1.5)**. Class I nAbs directly compete with the ACE-2 binding motif on RBD in the "up" conformation. Class II ACE-2 blocking nAbs bind both "up" and "down" RBD conformations and can contact adjacent RBD protomers. Class III neutralizing antibodies are classified as those that bind outside the ACE-2 site and recognize both the "up" and the "down" conformations of RBD. Class IV antibodies usually show weak neutralization and do not block ACE-2 (Barnes *et al.*, 2020).

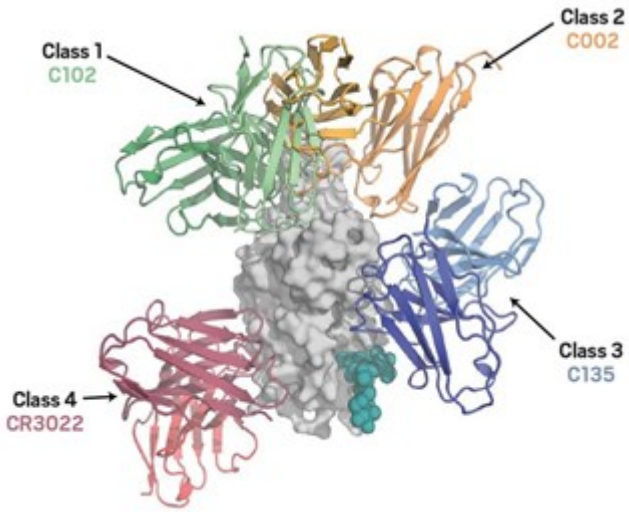

Figure 1. 5 Classification of antibodies based on location of epitope on RBD of the spike glycoprotein. Examples of each class of antibody are shown bound to different regions of the receptor-binding domain (gray).RBD Class I (light green) and Class II (orange) antibodies block the ACE-2 binding site. RBD Class III (navy blue) and Class IV (red) antibodies bind to sites outside the ACE-2 receptor binding site. Figure adapted from (Barnes *et al.*, 2020).

NTD-directed nAbs generally do not precisely block receptor binding (Zhou *et al.*, 2019) but rather obstruct with receptor binding by limiting spike protein conformational changes required for pre- to post-fusion transition (Fan *et al.*, 2020). The positively charged NTD supersite contains three loops referred to as N1 (residues 14–26), N3 (a β-hairpin formed by residues 140-158) and N5 (a loop spanning residues 245-264) (McCallum, De Marco, *et al.*, 2021) (**Figure 1.6**). SARS-CoV-2 NTD-directed nAbs are usually less potent than RBD-directed neutralizing antibodies. (Dai and Gao, 2021).

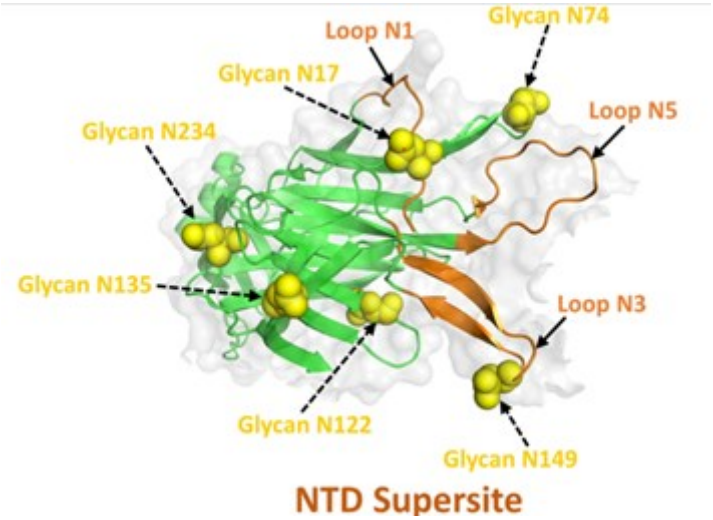

Figure 1. 6 Cryo-EM structure of SARS-CoV-2 NTD as a supersite for interaction. Structural representation of antigenic super- site of NTD (PBD id: 7L2C) in complex with a NTD binding antibody

shown in green. The NTD is surrounded by the N1, N3, and N5 loops shown in brown while glycans are shown as yellow spheres (Gupta *et al.*, 2021).

The conserved S2 subunit is also a target for antibodies that interfere with the structural re-organisation and the incorporation of fusion peptides mandatory for merging virus with host membrane (Chi *et al.*, 2020; Zhou *et al.*, 2022). The probability of mutations occuring in the S2 is relatively low and its conserved nature makes it an ideal target for a pan-betacoronavirus vaccine to induce antibody responses effective against VOC/VOIs and as well as to future coronavirus zoonoses (Burton and Topol, 2021; Koff and Berkley, 2021; Morens, Taubenberger and Fauci, 2022).

1.4.2 Antibody-dependent cellular cytotoxicity targeted against SARS-CoV-2 spike

The antiviral activity of antibodies is not limited to neutralization of viruses **(Figure 1.7)**. Infected cells opsonised by antibodies can be abolished through several non-neutralizing mechanisms, including antibody-dependent cellular cytotoxicity (ADCC), antibody-dependent cellular phagocytosis (ADCP) and antibody-dependent complement deposition (ADCD) (Dufloo *et al.*, 2021) **(Figure 1.7)**. ADCC is the cytotoxic reaction mediated by effector cells where target cells are perforated and destroyed (Pollara *et al.*, 2011; Ackerman *et al.*, 2013). During ADCC, antibodies cross-link SARS-CoV-2 antigens on the surface of infected cells and Fc receptors on effector cells which primarily consist of natural killer (NK) cells (Tauzin *et al.*, 2021) **(Figure 1.7)**. These Fc effector functions have been associated with reduced disease severity, mortality and associated with vaccine protection from infection in animal models (Zohar and Alter, 2020; Chan *et al.*, 2021; Schäfer *et al.*, 2021). Unlike neutralizing antibodies, which show reduced activity against VOCs, antibodies induced by both vaccination and infection that mediate ADCC are preserved against diverse variants (Kaplonek *et al.*, 2022; Richardson *et al.*, 2022).

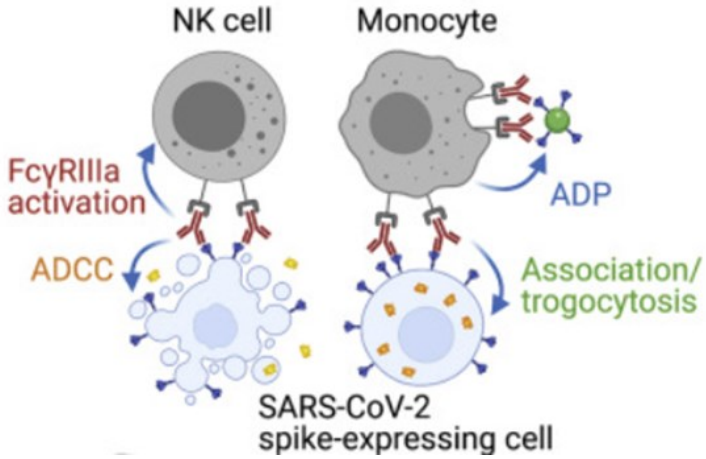

Figure 1. 7 Fc-mediated effector function. Graphical representation of antibody-antigen complex activating FcγRIIIa on NK cells mediating ADCC. Monocytes interact with Fc gamma receptors to stimulate and antibody-dependent phagocytosis (ADP) and trogocytosis, (Lee *et al.*, 2021).

1.5 SARS-CoV-2 variants of concern and interest

The continued evolution of SARS-CoV-2 since it was first discovered has led to the emergence of VOC/VOIs. The emergence of these variants has resulted in a greater risk to the population due to their high transmission risk, disease severity, immune pressure, treatment failure and/or reduced vaccine efficacy (Boehm *et al.*, 2021). The D614G mutation that emerged early in the pandemic and quickly became the dominant strain globally is now present in most circulating variants and is linked to increased viral transmission rates (Tegally *et al.*, 2021).

Mu is a highly resistant VOI against antibodies and is defined by the following mutations within the spike protein: T95I, Y144S, Y145N, R346K, E484K, N501Y, D614G, P681H and D950N (Tada *et al.*, 2021) **(Figure 1.8)**. Most of these mutations occurred in the RBD and NTD which are the primary targets of neutralizing antibodies. Some mutations in Mu are commonly identified in other VOCs such as Beta, Gamma and Omicron and have shown reduction in sensitivity to antibodies induced by SARS-CoV-2 infection and vaccination (Uriu *et al.*, 2021). Understanding how the spike protein evolves as it mutates and escapes antibody responses is crucial to vaccine design. Furthermore analyses of antibody responses towards neutralization resistant Mu variant may provide unique insights into the qualitatively different antibody binding and cross-neutralizing activity imprinted by different variant spikes.

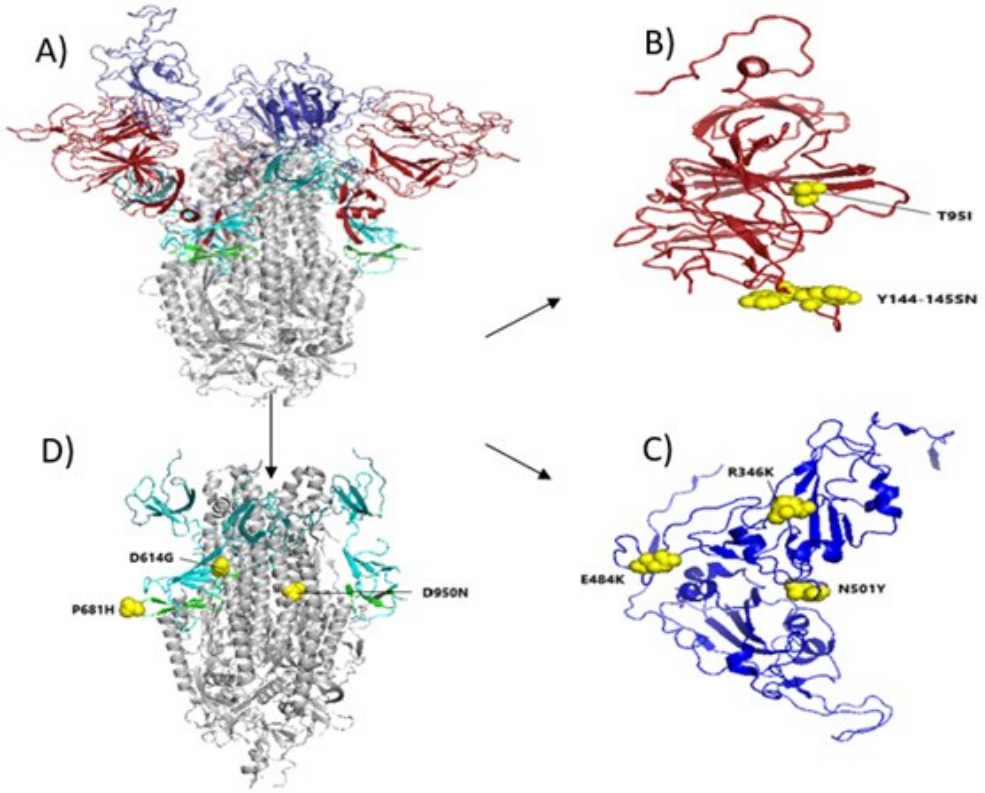

Figure 1. 8 CryoEM structure of SARS-Cov-2 Mu variant. Spike protein with open confirmation. The NTD shown in red, RBD in blue, SD1 in teal, SD2 in cyan and S2 region shown in gray. **B)** A close up of the NTD with mu defining NTD mutations shown in yellow. **C)** A close up of the RBD with mu defining mutations shown in yellow **D)** Mu defining mutations from other regions of the spike. Pymol version 2.4.1 was used for analysis of protein structure (PDB ID:7WZ2) obtained from the protein biobank

Mu shares the RBD N501Y mutation associated with increased transmissibility with four variants of concern: Gamma (P.1) first identified in Brazil (Wang *et al.*, 2021), Alpha (B.1.1.7) first identified in United Kingdom (Khoury *et al.*, 2021), Beta (B1.351) and Omicron (B.1.1.52) first identified in South Africa (Boehm *et al.*, 2021; Viana *et al.*, 2022). This mutation results in greater affinity to the human ACE2 receptor. The E484K mutation found in Beta, C.1.2, Gamma, Iota and Eta variants is associated with decreased neutralization, leading to reduced *in vitro* efficacy of some antibody therapies or vaccines (Greaney *et al.*, 2021). The R346K mutation found in both Mu and Omicron abrogates binding of class II antibodies (Fratev, 2021).

The furin cleavage site P681H mutation in Mu (also found in Alpha and Omicron) has been shown to enhance cleavage at the S1-S2 boundary, improve cell-cell fusion and increase virus replicative fitness (Liu *et al.*, 2021). Mu also contains the T95I substitution outside the NTD

antigenic supersite which has not been shown to contribute substantially to immune evasion (McCallum *et al.*, 2021). The D950N mutation in Mu was mapped to the trimer interface suggesting that this mutation may contribute to the regulation of spike protein dynamics, similarly to the D614G mutation (Plante *et al.*, 2021). While the Mu lineage shares common mutations with other VOC/VOIs, it also has a number of unique mutations - Y144S and Y145N - that have unknown impact on immune escape or virus replicative fitness (**Figure 1.8**).

1.6 SARS-CoV-2 vaccine efficacy against variants of concern

Multiple COVID-19 vaccines have been tested in pre-clinical and clinical trial settings, some of which are highlighted in **Table 1.1**. When tested against the D614G strain, most vaccines induced robust humoral and cellular responses and lowered the risk of acquisition of severe COVID-19 (Baden *et al.*, 2020; Polack *et al.*, 2020; Alter *et al.*, 2021).

mRNA vaccines such as mRNA-1273 (Moderna) and BNT162b2 (Pfizer) demonstrated over 90% efficacy against acquisition of SARS-CoV-2 in clinical settings with the D614G strain (Gómez, Perdiguero and Esteban, 2021), while viral vector vaccines such as Ad26.COV2.S (Johnson & Johnson) and AZD1222 (ChAdOx1; Oxford/Astra-Zeneca) showed efficacies of above 60% (Alter *et al.*, 2021; Voysey *et al.*, 2021).

However, emergence of the Beta strain decreased vaccine efficacy for Ad26.COV2.S and AZD1222 with efficacies dropping to 52% and 22% respectively depending on the region or country in which they were tested (Madhi *et al.*, 2021; Sadoff *et al.*, 2022). Despite the reduced prevention efficacy, the vaccines were shown to retain effectiveness in prevention of severe disease.

Heterologous vaccine prime-boost strategies have been studied. Atmar *et al*., 2022 demonstrated that heterologous boosting with either BNT162b2, AZD1222 or Ad26.COV2.S induced robust immune response which resulted in substantial increases in binding antibodies and neutralizing antibodies. Borobia *et al*., 2021, demonstrated that BNT162b2 given as a second dose in individuals vaccinated with AZD1222 induced significantly higher immune responses in the heterologous vaccination arm than the control vaccination arm. The effect of

break-through infections in vaccinated individuals has been studied and shown to lead to an increase of specific antibodies in serum and saliva (Kitchin *et al.*, 2022; Terreri *et al.*, 2022).

Table 1. 1 SARS-CoV-2 vaccines efficacy against SARS-CoV-2 VOCs

Vaccine code name and	Vaccine Type	Efficacy against WT	Vaccine Efficacy/Effectiveness against VOC infection	
AZD1222 (Astrazeneca)	Viral Vector	62.6%	Alpha	37% (Sheikh *et al.*, 2021)
			Beta	22% (Madhi *et al.*, 2021)
			Delta	67% (Bernal *et al.*, 2021)
Ad26.COV2.S Johnson & Johnson	Viral Vector	66%	Alpha	70% (Sadoff *et al.*, 2022)
			Beta	51.9% (Sadoff *et al.*, 2022)
			Delta	51% (Barlow, Jian and Larson, 2021)
BNT162b2 Pfizer/BioNTech	mRNA	95%	Alpha	89% (Nasreen *et al.*, 2021)
			Beta	75% (Abu-Raddad, Chemaitelly and Butt, 2021)
			Gamma	84% (Nasreen *et al.*, 2021)
			Delta	89% (Tang *et al.*, 2021)
			Omicron	70% (Collie *et al.*, 2021)
mRNA-1273 Moderna	mRNA	95%	Alpha	92% (Nasreen *et al.*, 2021)
			Beta	96% (Chemaitelly *et al.*, 2021)
			Delta	80.2% (Tseng *et al.*, 2022)
			Omicron	44% (Tseng *et al.*, 2022)
NVX-CoV2373 Novavax	Recombinant protein	90%	Alpha	86.3% (Heath *et al.*, 2021)
			Beta	51% (Shinde *et al.*, 2021)

There are limited studies examining vaccine effectiveness against Mu, however a trial by Bruxvoort *et al* using a two dose vaccine regime of mRNA-1273 reported vaccine effectiveness of 90.4% against infection with Mu variant (Bruxvoort *et al.*, 2021). Studies conducted using vaccinee plasma from donors immunized with either BNT162b2, Ad26.COV2.S or mRNA-1273 showed a reduction in neutralization, with fold decreases between 6.8 and 7.3 (Tada *et al.*, 2022).

1.8 Aims and Objectives

Study rationale

Due to the accelerated evolution of SARS-CoV-2 mutations and the emergence of VOC/VOIs, there is an urgent and continued need to study the humoral response against SARS-CoV-2

variants to facilitate the advancement of next-generation vaccines and curative strategies. There is substantial data that shows that different variants trigger qualitatively different neutralizing and Fc effector specificities (Keeton *et al.*, 2021; Moyo-Gwete *et al.*, 2021; Richardson *et al.*, 2022), providing a rationale to study neutralization and Fc effector function resistance following infection by different variants. As many VOC/VOIs share common mutations, defining the resistance of less characterised variants, such as Mu, provides a useful tool for mapping neutralizing and other antibody specificities in convalescent donors. This may aid in the identification of conserved epitopes to use in the design of variant-based vaccines.

In this study, we assessed antibody responses elicited by four variants (WT D614G, Beta, Delta and Omicron (BA.1)) during four waves of COVID-19 infection experienced in South Africa. We used convalescent sera to measure binding, neutralization and ADCC activity against Mu, and compared responses across each of the waves. This study sought to determine whether there was differential targeting of Mu by defining and mapping the targets of humoral responses triggered by different variants. As Mu shares many features with other VOCs, this may aid in predicting the impact of mutations that may be common to emerging VOCs.

Aim: This study aimed to assess the functional capacity of antibodies in plasma from infections by four distinct SARS-CoV-2 variants against the Mu variant to identify cross-reactive antibodies. Defining their epitopes may provide templates for rational immunogen design strategies for next-generation vaccines.

Objective 1: To assess cross-neutralizing activity of plasma from convalescent donors infected with WT D614G, Beta, Delta or Omicron (BA.1) against the Mu variant

Objective 2: To identify mutations in key regions that mediate neutralization escape in Mu.

Objective 3: To measure ADCC activity in convalescent plasma from four waves of infection against Mu.

2. Materials and Methods

2.1 Ethical Considerations and Study Cohorts

A total of seventy five plasma samples from participants with varying disease severity were used for this study. Wave 1 plasma samples were obtained from D614G-infected patients admitted at the Steve Biko Hospital, Tshwane with symptom onset between May and August 2020. Plasma samples from waves 2 onwards were obtained from SARS-CoV-2 infected patients admitted to Groote Schuur Hospital, Cape Town during the second, third and fourth COVID-19 waves in South Africa. Second wave (Beta-infected) samples were collected in December 2020 - January 2021, third wave (Delta-infected) samples were collected July – August 2021 while fourth wave (Omicron) samples were collected December 2021- January 2022 **(Table 2.1)**. The median ages were comparable between the different waves (47-59 years). Enrolment was based on the following criteria: a polymerase chain reaction (PCR) confirmed SARS-CoV-2 infection, age ≥18 years and HIV negative status. Written and informed consent was obtained from all participants. Participant clinical folders were consulted and there was no evidence of prior symptomatic COVID-19 infection.

Table 2. 1 Demographic characteristics of study participants

Infecting variant	Cohort	Sample polulation	Sample collection period	Median age (range)	Sequence confirmed	Average days post	Female: male
WT D614G	Steve Biko (Wave 1)	17	May 2020-Aug 2020	51 (26-72)	0	11	06:11
Beta	GSH (Wave 2)	18	Dec 2020-Jan 2021	59 (48-83	4	7	11:07
Delta	GSH (Wave 3)	22	July 2021	47 (22-76)	8	7	14:08
Omicron	GSH (Wave 4	18	Dec 2021-Jan 2022	51 (21-77)	6	4	11:07

Ethical clearance for this study was obtained from the Human Research Ethics Committee (HREC) of the University of the Witwatersrand (Ethics number: M211142). The parental study from the Groote Schuur Hospital cohort received ethical approval from the Human Research Ethics Committee of the Faculty of Health Sciences, University of Cape Town (Ethics number: R021/2020). Ethical approval for the Steve Biko Cohort was received from the University of Pretoria, Human Research Ethics Committee (Medical) (Ethics number: 247/2020).

2.2 Site Directed Mutagenesis of SARS-CoV-2 Mu Spike

To introduce the Mu variant specific mutations of interest into both pseudoviruses and soluble protein antigens, the viral envelope DNA of WT D614G spike was used as a template. Primers were designed to introduce mutations in a single step polymerase chain reaction (PCR) **(Table 2.2)**. Site-directed mutagenesis was performed using the Lightning Site Directed Mutagenesis kit (Agilent Technologies) as per manufacturer's instruction, which works by using a double stranded pcDNA3.1 vector with the insert of interest. In this case the insert was the SARS-CoV-2 envelope glycoprotein gene. Synthetic oligonucleotide primers were used, each complementary to one strand of the insert DNA, both containing the desired mutations.

Table 2. 2 List of primer sequences

Primer Name	SEQUENCE (5' – 3')
Mutagenesis Primers	
T95I	GATGTTGGACTTCTCGATAGAGGCGAAATACACGC
Y144S+Y145N	GATCCCTTCCTGGGCGTGTCCAATCATAAGAACAATAAGTCC
R346K	GCGAGGTGTTCAACGCTACCAAGTTCGCCTCCGTGTACG
E484K	CCCCTTGCAATGGCGTGAAGGGCTTTAACTGTTATTTC
N501Y	CTTCCAGCCCACATACGGCGTGGGCTATC
P681H	GACCTGGCCCTCCTGTGAGAGTTTGTCTGGG
D950N	TTCTGATTCACCACATTCTGGAGCTTGCCCAGG

Cycling parameters were set as provided by the kit manufacturer **(Table 2.3)**. Cycling conditions involved cleavage by a restriction enzyme at a site in the plasmid, subsequent ligation of a pair of complementary oligonucleotides containing the mutations in the gene of interest to the plasmid and elongation of the produced mutant plasmids. Following temperature cycling, 1µl of Dpn-1 endonuclease restriction enzyme (target sequence 5'- Gm6AT-3') was added directly to each amplification reaction at 37°C for 2 hours to digest parental non-mutated dsDNA. The enzyme works by specifically selecting for methylated or hemi-methylated DNA.

Table 2. 3 The Quickchange Site Directed Mutagenesis thermal cycling conditions used introducing spike mutations

Segment	Cycles	Temperature	Time
Initial denaturation	1x	95°C	2 minutes
Denaturation	30x	95°C	20 seconds
Annealing		55°C	30 seconds
Extension		65°C	4 minutes
Final extension	1x	68°C	5 minutes
Hold	1x	4°C	∞

2.3 Transformation of XL-10 Gold Ultracompetent E. Coli Cells

XL10 Gold Ultra-competent *E. coli* cells (Agilent technologies) were transformed to clone the desired DNA plasmid. β-mercaptoethanol was added to the cells to denature RNAses by reducing disulfide bonds that may affect efficacy of the transformation. 50ng of the cloned viral DNA together with 50µl of cells were added to pre-chilled tubes. The cells were subjected to heat shaking at 42°C for 30 seconds in a water bath to expand bacterial membranes and thus allow DNA into the cells. Cells were recovered in a nutrient-rich super optimal broth with catabolite suppression (SOC) medium for one hour at 37°C with shaking at 200 rpm. Thereafter the cells were plated to select for single colonies on Luria Bertani (LB) Agar supplemented with 100µg/mL kanamycin for protein spike and carbenicillin for pseudovirus at 37°C overnight. Subsequently, four single colonies of cells were picked and cultured in 250mL LB broth and incubated overnight at 37ºC in a shaking incubator (200 rpm) for large scale DNA preparations while small scale were cultured in 5mL LB Broth.

2.4 Production of small-scale plasmid preps from transformed cells

Plasmid DNA extraction from bacterial cells was performed using the Qiagen QIAprep® spin mini prep kit for spike plasmid preparations. The bacterial culture was pelleted at 5 000 rpm for ten minutes and the supernatant discarded. The bacterial pellet was resuspended in 250µl of resuspension buffer. A volume of 250µl of lysis buffer was added to the pelleted cells. A volume of 350µl neutralization buffer was added to stop the lysis process and optimize conditions for DNA binding onto the silica membrane column. The bacterial lysate was pelleted by centrifuged at 13 000 rpm for ten minutes and DNA collected from the supernatant

was added to a spin column to bind the DNA onto the membrane. To remove any endonucleases, 250µl of wash buffer was used to wash the membrane bound DNA. This was followed by another wash step with 750µl of a second wash buffer to remove excess salts or contaminants on the membrane. The membrane bound DNA was recovered by elution in 50µl elution buffer and quantified on a NanoDrop™-1000 Spectrophotometer (Thermo Scientific).

2.5 Production of large-scale plasmid preps from cloned envelopes

Large-scale preparations of each of the cloned hexapro spike envelopes were produced using the ZymoPURE™ maxi prep kit. The bacterial culture was pelleted at 5 000 rpm for fifteen minutes and the LB supernatant discarded. The bacterial pellet was re-suspended in 14ml of re-suspension buffer P1. Bacterial culture was lysed under alkaline conditions using lysis buffer P2. The lysate was neutralized by adding 14ml neutralization buffer P3. The mix of dissolved DNA and lysed cells was spun for 10 minutes for the lysate to float. A ZymoPURE™ Syringe Filter-X was used to filter the DNA rich supernatant. The supernatant was loaded onto Zymo-Spin™ V-PX column and a volume of 14ml of ZymoPURE™ Binding Buffer was added. subsequently the DNA was eluted in 400µl buffer ZymoPURE™ Elution Buffer and quantified on a NanoDrop™-1000 Spectrophotometer (Thermo Scientific). The spectrophotometer was blanked using 2µl of the elution buffer and the concentration of DNA was measured using 2µl of the DNA solution.

2.6 Sanger Sequencing of Mu spike plasmids

The successful introduction of mutations was verified using Sanger sequencing with the Applied Biosystems Big Dye sequencing kit. Site specific primers along the spike protein were used to perform sequencing. To sequence the full spike gene, a set of overlapping primers were used (**Table 2.4**).

Table 2.4 List of sequencing primers

	Primer Name	SEQUENCE (5' – 3')
	Sequencing Primers	
Mu Pseudovirus spike	seq300-R	CACGATCAGCAGAGACTGTGTC
	>SARS2-S-seq700-R	GTTGATGCCGATAGGCAGATCC
	>SARS2-S-seq2500-F	GCTTCATCAAGCAGTATGGC
	>SARS2-S-seq3200-F	GCTATCACCTGATGAGCTTCC
	>SARS2-S-seq3700-R	GCATGATGGTCACCATCACG
	SARS2-S-seq400	CAACGTGGTCATCAAGGTGTGCGAG
	SARS2-S-seq800	CGCTGGCGCCGCTGCCTAC
	SARS2-S-seq1200	CGCTGATTCTTTCGTGATCAGAGGCG
SARS1 Mu Chimera's	Delta 28 R2	GTGTTGTTGCTGTAGGCAATG C
	Delta 28 F2	GGCTACCTGAAACCAACCACC
	Delta 28 F1	GAATACATCTCTGATGCCTTC
	Delta 28 R1	GGGTTCTGGCTACAGTCC A
	Delta 28 F3	CCATGTACTCCTCCTGCCC
	Delta 28 F4	GGAGCACCAGCCAGAAGAGC
	Delta 28 F5	GGCTCTGAACACCCTGGTG
	Delta 28 F6	GTGTCTGGCAACTGTGATG
	Delta 28 R3	CTCAGCCTCCACCTTGTCC

Sequencing reactions were set according to manufacturer's recommendations **(Table 2.5**).

Table 2.5 Cycling conditions for Sanger sequencing using the Big dye terminator kit

Segment	Cycles	Temperature	Time
Initial	1x	96°C	1 minutes
Denaturation	25x	96°C	10 seconds
Annealing		50°C	5 seconds
Extension		65°C	4 minutes
Hold	1x	4°C	∞

The sequencing reaction set up was done according to the manufacturer's specifications (Adapted from Applied Biosystems).

Table 2.6 Sanger sequencing

Component	Diluted reaction (0.5X)		
	Quantity per reaction	Example Forward	Example Reverse
BigDye™ Terminator 3.1 Ready Reaction Mix	4µL	4µL	4µL
BigDye™ Terminator v1.1 & v3.1 5X Sequencing Buffer	2µL	2µL	2µL
Forward primer (3.2 µM)	3.2pmol	2µL	—
Reverse primer (3.2 µM)		—	2µL
Deionized water (RNase/DNase-free)	*	10µL	10µL
Template	300ng	2µL	2 µL
Total volume	20 µL	20 µL	20 µL

After cycling, sequencing reactions were cleaned to remove any salts and impurities according to the manufacturer's specifications (**Table 2.6**). Sequence clean-up was done by precipitating sequencing reaction products by adding 300µl of 3M sodium acetate to 8ml of 99% ethanol. A total of 50µl of the mixture was added to each well of 96 well plate, the plates were then centrifuged for 30 minutes at 2 000 rpm. Supernatant was removed by inverting the plate and spinning it at 150 rpm for one minute. Cold 70% ethanol was added to each well at a volume of 100µl and the plate spun at 2 000 rpm for five minutes. The supernatant was removed by inverting the plate and spinning it at 150 rpm for one minute. The reactions were dried on a PCR machine at 65°C for 3 minutes. Cleaned pellets containing 10ul HiDi formamide (Applied Biosciences) were run on the ABI Prism® 3500xl Genetic Analyser.

Sequences from the Genetic Analyser were analyzed using Sequencher 5.4.6 software (Gene Codes Corporation). Sequences were analysed by aligning the resultant mutated sequence of Mu to the reference (non-mutated) WT D614G sequence to confirm the insertion of the desired mutations. Sequences of poor quality showing double peaks on the chromatogram were disregarded.

2.7 Maintenance of mammalian cell lines

Human embryonic kidney cells (HEK293T) were obtained from NIH AIDS Research and Reference Reagent Program and were used for the transfection of pseudoviruses. The 293Freestyle cells were used to express spike antigen, and were obtained from the Vaccine Research Center, USA. HEK293T ACE-2 expressing cells and Jurkat-Lucia™ NFAT-CD16

cells were supplied by Dr Michael Farzan and were used for antibody neutralization assays as mentioned.

Dulbecco's Modified Eagle's Medium (DMEM) supplemented with 10% fetal bovine serum (FBS), 2.5% HEPES buffer and 50µg/ml gentamicin was used to maintain HEK293T cells. Cells were grown at 37°C, 5% CO2 and disrupted at 80% or more confluence with 0.25% trypsin every 48–72 hours.

HEK293T ACE-2 cells were maintained in DMEM supplemented with 3µg/ml of puromycin, 10% fetal bovine serum (FBS), 2.5% HEPES buffer and 50µg/ml gentamicin. The cells were cultured at 37°C, 5% CO2, maintained by splitting and seeding when they reach a confluence of 80%. The 293Freestyle cells were cultured in a shaking incubator at 37°C, 5% CO2, 70% humidity at 125 rpm. 293Freestyle cells were maintained in 293Freestyle media and diluted every 72 hours in order to keep the concentration below $3x10^6$ cells per millilitre.

The Jurkat-Lucia™ NFAT-CD16 cells were cultured at 37°C, 5% CO2 and maintained in Iscove's Modified Dulbecco's Medium (IMDM) supplemented with 10% FBS, 1% Pennicillin-streptomycin, 10µg/ml of Blastocydin and 100µg/ml of Zeocin was added to the growth medium every other passage. Cells were diluted every 48 hours to keep cell concentration at 500 000 cells per millilitre.

2.8 Expression of soluble full spike

SARS-Cov-2 Mu, Mu RBD or Mu NTD spike antigen was expressed in HEK293F suspension cells seeded at $1x10^6$ cells/ml at 37°C in a shaking incubator a day prior to transfection. Serum free Optipro media (Thermo Fisher Scientific) together with 500µg of purified SARS-CoV-2 DNA plasmid produced was filtered using a 0.2µm filter into freshly prepared PEI-MAX (Polyethyleneimine) transfection reagent mixed with Optipro and incubated for 20 minutes at room temperature. After incubation, the mixture was added to the HEK293F cells and the cells were incubated shaking for 6-7 days at 37°C, 10% CO2, 70% humidity.

2.9 Protein purification using affinity and size exclusion chromatography

Cell culture supernatants containing the SARS-CoV-2 Mu, Mu RBD or Mu NTD spike protein were spun down at 4 000 rpm to pellet cells then filtered through 0.22µm Vacuum Filtration-Filtermax flasks (TPP; Trasadingen). The filtrate was then passed through a nickel-affinity column and a wash buffer (20mM Imidazole, 20mM Tris-HCl, 150mM NaCl) was used to remove unwanted proteins. Approximately 20ml of eluent was collected using an elution buffer consisting of 20mM Tris-HCl, 400mM Imidazole and 150mM NaCl and concentrated using a 50 kDa Vivaspin® protein concentrator (Sartorius stedim). The concentrated spike proteins were further purified using size exclusion chromatography (SEC) on a Superdex 200 column (HiLoad 16/600, Cytiva) which separates proteins based on molecular weight. The SARS-CoV-2 spike fractions eluted at 42 – 55 minutes were collected and concentrated. Aliquots were stored at - 80°C until use.

2.10 Enzyme linked immunosorbent assay

A SARS-CoV-2 enzyme linked immunosorbent assay (ELISA) was used to measure spike binding antibodies in convalescent plasma and antibody cross-reactivity to the Mu variant. High-binding 96 well plates (Thermo Fisher Scientific) were coated with 50µl of 2µg/ml diluted SARS-CoV-2 spike antigen per well a day prior to running the experiment. Each plate was sealed with clear plate sealers and incubated in a 4°C fridge overnight. On the next day, the plate was washed 3 times with 250µl wash buffer consisting of 1xPBS and 0.05% tween using an automated plate washer. A volume of 200µl blocking buffer (5% non-fat milk in wash buffer) was added to all wells and incubated at room temperature for 1 hour. Plates were washed 3 times with 250µl per well of wash buffer using an automated plate washer. 1:100 dilutions of plasma samples were prepared. Positive and negative control monoclonal antibodies were diluted to a 5µg/ml starting concentration. The prepared sample or antibody dilutions were added and titrated down the plate in 3-fold dilutions. Plates were then incubated at room temperature for 1 hour 30 minutes. After incubation, the plates were washed and 100µl of secondary antibody that was diluted at 1:3 000 in blocking buffer was added. Plates were incubated for an hour followed by a wash step. In a dark hood, 100 µl 1-step tetramethylbenzidine (TMB) substrate was added to all the wells and incubated at room temperature covered in foil for 5 minutes until the plates developed. The reaction was stopped

by adding 50µl 1M H_2SO_4 to all the wells. Plates were read immediately at a wavelength of 450nm on the plate reader. Area under the curve was determined for each sample. Friedman's test with Dunn's correction to calculate statistical differences using Graphpad Prism version 8.

2.11 Production of SARS-CoV-2 pseudoviruses

HEK293T cells were seeded in 12 ml DMEM at $6x10^6$cells in a T75 flask 24 hours prior to transfection to achieve approximately 60-80% confluency. The cloned SARS-CoV-2 spike plasmids (mutant and WT spikes) and HIV pNL4-3 backbone that possessed package expression cassettes for firefly luciferase were co-transfected into the cells. An amount of 10µg of spike plasmid and 10µg of the pNL4-3 vector was combined with 500µl serum free DMEM and 48µl of the transfection reagent PEI-MAX. The mixture was incubated at room temperature for 30 minutes to allow the formation of transfection complexes. After incubation the transfection mixture was added to the cells and incubated for 72 hours. The supernatant containing the pseudoviruses was harvested after 72 hours and 20% FBS was added to preserve the virus. The pseudovirus preparation was filter-sterilized using a 0.45um filter and stored at -80 degrees until use.

2.12 Titration of SARS-CoV-2 pseudoviruses

The amount of virus in the supernatant was determined by titration of the virus using HEK293T cells engineered to express ACE-2. In a 96 well flat bottom plate, 100µl of supplemented DMEM was added to each well. A volume 50µl of the pseudovirus was added to row A, except into the background controls. A total volume of 50µl was titrated down the plate and after dilution, 100µl of HEK239T ACE-2 cells were added to each well and incubated for 72 hours. The infected cells express luciferase and luciferase activity is quantified by relative light units (RLU) of luminescence. The luminescence is directly proportional to the number of infectious viral particles.

2.13 SARS-CoV-2 neutralization assay

This assay measures neutralization of SARS-COV-2 as a function of reduction in expression of luciferase reporter gene after a single round of infection in HEK293T ACE-2 cells

engineered to express ACE-2 (Neerukonda *et al.*, 2021). Neutralization assays were performed on a 96 well plate where five samples were titrated in duplicate per plate to assess neutralizing antibody responses elicited against different pseudotyped spikes.

Plasma samples added in duplicate were serially diluted with DMEM in a 96-well plate, and co-incubated in a total volume of 150µL for one hour at 37°C with pseudovirus at a concentration previously determined to yield 40 000 RLUs. To each well 100µL of HEK293T ACE-2 cells were added to a final concentration of $1x10^6$ cells per plate, and further incubated for 72 hours at 37°C, 5% CO_2 to allow pseudovirus infection.

Thirty µl of 1x promega lysis buffer was added to all wells and incubated for 10 minutes at room temperature for cell lysis to take place. A volume of 100µl of luciferase was added and incubated for 2 minutes to allow the reaction between the enzyme and substrate to take place. The reaction was transferred to a black/white plate and luminescence was read on a Perkin Elmer Victor X luminometer. Infected cells expressed luciferase and neutralization was measured using a fluorescence based system where the amount of virus neutralized was indicated by the reduction of level of fluorescence in each well. The 50% inhibitory dilution (ID_{50}) will be defined as the serum dilution at which the RLUs are reduced by 50% compared with the virus control wells. The ID_{50} values of all samples were plotted using GraphPad Prism version 8.

2.14 Spike expression on the surface of HEK293T cells

Prior to testing the ability of antibodies to mediate antibody dependent cellular cytotoxicity (ADCC), spike-transfected HEK293T cells were tested to confirm the expression of the SARS-CoV-2 spike variants on the cell surface. Target cells were generated by transiently transfecting HEK293T cells in a petri dish with 5µg SARS-CoV-2 Mu or WT D614G spike three days prior to performing the experiment. A set of positive control antibodies known to bind to WT D614G or Mu spike equivalently were co-cultured at 100µg/ml in a 96 well plate with the transfected cells for 20 minutes at room temperature. This includes AIRU946-A6, CB6 and lastly P2B which differentially bind to the spike variants. Non-transfected HEK293T, as well as Palivizumab which is a RSV specific mAb that does not bind to WT D614G and Mu spike, were added as negative controls while in some wells no antibody was added to the cells to

account for the background of the assay. To detect binding of the antibodies to the expressed spikes, a 1:100 dilution of an Fc region IgG-specific secondary antibody conjugated to APC, was added to the culture and incubated for 15 minutes at room temperature. Two wash steps with 200µl of 1x PBS per well followed and the cells were fixed with 4% paraformaldehyde (PFA) until the plates were acquired in the Alexa-Flour-647 channel on the FACSAriaII flow cytometer (BD Biosciences; Franklin Lakes, USA). The mean Alexa-Flour-647 fluorescence intensity of each transfected spike variant bound to AIRU946-A6 relative to the no antibody control and non-transfected HEK293T cells was then determined through analysis on the FlowJo™ 10 Software as a measure of spike expression.

2.15 Antibody-dependent cell-mediated cytotoxicity (ADCC) assay

The ADCC potential of the plasma was evaluated as their capacity to cross-link and activate the FcγRIIIa (CD16) receptor on the surface of the Jurkat-Lucia™ cell line in the presence of spike expressing cells, as a proxy for ADCC. In a 96 well tissue culture treated plate convalescent plasma at a dilution of 1:100 was added and incubated for 1 hour at 37°C, 5% CO_2 together with the spike-transfected cells. Subsequently, $2x10^5$ Jurkat-Lucia™ NFAT-CD16 cells per well were added and incubated at 37°C, 5% CO_2 for 24 hours. To induce the transgene 1x cell stimulation cocktail (Thermo Scientific) and 2µg/ml ionomycin in R10 was also added as a positive control to confirm sufficient expression of the CD16 Fc receptor. ADCC was measured as the increase in luciferase activity measured in Relative light units (RLU) compared to the no plasma control. To measure RLUs, 20µl of supernatant was transferred to a white 96-well plate with 50µl reconstituted QUANTI-Luc secreted luciferase and read immediately in triplicate. The reported values are the mean of three kinetic reads taken.

3. Results

3.1 SARS-CoV-2 spike protein expression and purification

SARS-CoV-2 spike proteins were expressed and purified for use in determining the presence of binding antibodies in convalescent plasma. The SARS-CoV-2 Mu plasmid was transfected into HEK293F cells and the expressed spikes were harvested from supernatant after seven days. The fractions eluted at 42 – 55 minutes were collected (**Figure 3.1A**) and concentrated as the SARS-CoV-2 spike. Spectrophotometry was used to quantify the amount of spike obtained which was 2.1mg for Mu. The expression level of Mu spike was compared to a previous batch of WT D614G (**Figure 3.1A**). The Mu spike was successfully expressed as confirmed by SDS-PAGE and SEC profile (**Figure 3.1**).

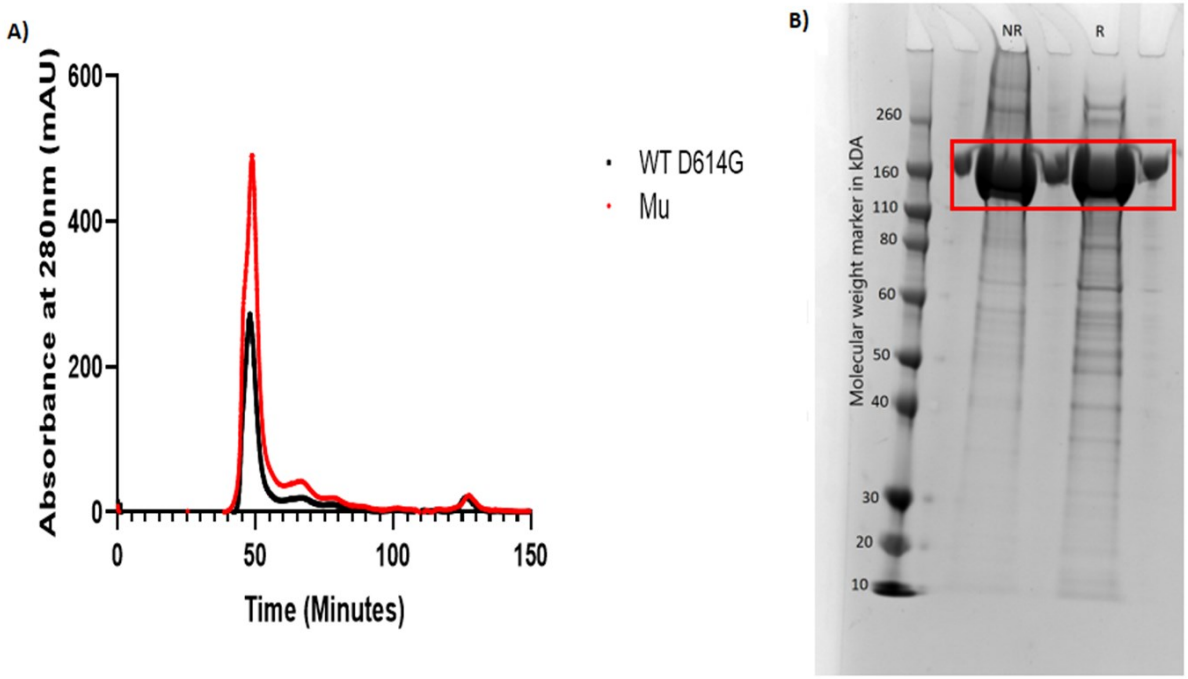

Figure 3. 1 SARS-CoV-2 Mu protein size exclusion chromatography profiles and SDS-PAGE to confirm purity of the spike protein. (A) Mu spike proteins are represented by red superimposed on WT D614G spike represented by black. The x-axis shows the time each fraction was eluted while the y-axis shows the relative amount of protein that was eluted at each time point (B) A non-reducing (NR) and Reducing (R) SDS PAGE gel showing the expressed Mu spike protein compared to a known molecular weight protein marker in kDa.

The purity and size of spike proteins was confirmed by a reducing and non-reducing SDS-PAGE gel. The bands on the gel confirmed that the spike protein was the expected size of approximately 160 kDa, with minimal impurities (**Figure 3.1B).**

3.2 Antibodies elicited by variants of concern retained cross-reactive binding responses targeting the Mu variant

The consequence of Mu mutations on binding of SARS-CoV-2 directed antibodies was assessed by ELISA. Plasma samples were obtained from participants infected with either WT D614G, Beta, Delta or BA.1. Binding was plotted as the area under the curve for each sample (**Figure 3.2)**. Binding antibody responses were generally higher towards the infecting variants than Mu, with Delta exhibiting the highest level of autologous binding (GMT: 6724) followed by WT D614G (GMT: 6449), while BA.1 and Beta elicited lower levels of autologous binding responses (GMT: 2295 and 1424, respectively). The fold loss of cross-reactive binding responses varied per variant (**Figure 3.3**). Beta displayed the highest level of cross-reactive binding to Mu with GMT of 3699 and BA.1 retained a relatively high level of cross-reactive binding to Mu with GMT of 2447 similar to the infecting variant. In contrast, WT D614G and Delta displayed approximately 3-fold drops in binding antibodies targeting the Mu variant with GMTs of 2406 and 2076, respectively.

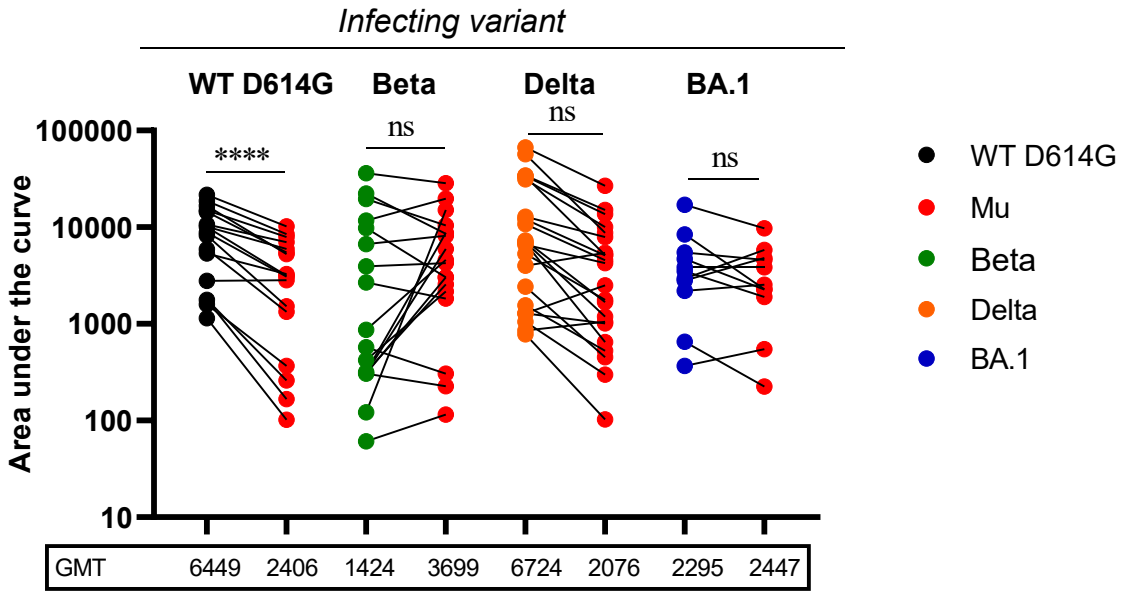

Figure 3. 2 Binding antibody responses against WT D614G and Mu spike proteins. Binding in convalescent plasma from infection with D614G (black), Beta (green), Delta (orange) and BA.1 (blue).

Binding was tested in a three-fold serial dilution starting at 1:100. Plasma was tested against the autologous virus and Mu, binding is represented as area under the curve. Geometric mean titers are also shown below the plot. Statistical significance was calculated using the Friedman test with Dunn's correction. *p<0.05; **p<0.01; ***p<0.001; ****p<0.0001 and ns = non-significant.

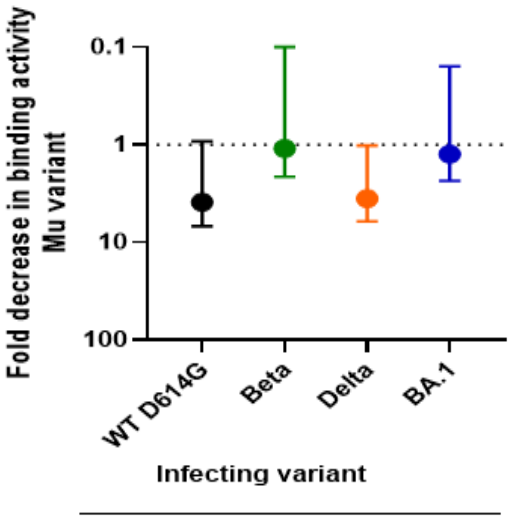

Figure 3. 3 Fold difference represented as binding activity. Fold reduction in binding is shown as the proportion of the binding to Mu variant compared to the infecting variant. No difference in fold changes is represented by the dotted line. GMTs were calculated for each group and the fold change relative to Mu binding is shown.

Samples obtained from WT D614G or Delta infection showed less cross-reactivity against Mu, with a greater than two-fold reduction in binding (3.1 and 2.8, respectively) while samples from infection with Beta and BA.1 showed the least binding escape with fold changes of 0.4 and 0.9, respectively (**Figure 3.3**). All variants elicited cross-reactive binding antibodies although the magnitude of binding to Mu was reduced by an average fold drop of 1.8 (**Figure 3.3**).

3.3 The Mu variant escapes neutralization by monoclonal antibodies

We further assessed the neutralization sensitivity of Mu to mAbs as this would aid in determining Mu resistance profiles and in mapping sites of vulnerability. Several mAbs from different antibody classes, targeting either the NTD or RBD, were tested head to head against the WT D614G and Mu using the pseudovirus neutralization assay. WT D614G was used as a control for this experiment as neutralization sensitivity towards this variant had already been determined for these mAbs (Yang *et al.*, 2020; Corti *et al.*, 2021; Fouladirad and Bach, 2021; Weinreich *et al.*, 2021). All the antibodies known to neutralize WT D614G neutralized the

virus as expected, with IC_{50} values that were highly concordant with historic data (Chi *et al.*, 2020; Ju *et al.*, 2020; Pinto *et al.*, 2020; Shi *et al.*, 2020; Starr *et al.*, 2021; Wibmer *et al.*, 2021). All mAbs that failed to neutralize the WT D614G virus in this experiment were shown to be resistant to the WT D614G from previous inhouse experiments and published data (Rogers *et al.*, 2020; Moyo-Gwete *et al.*, 2022). This confirmed the neutralization capacity of the mAbs.

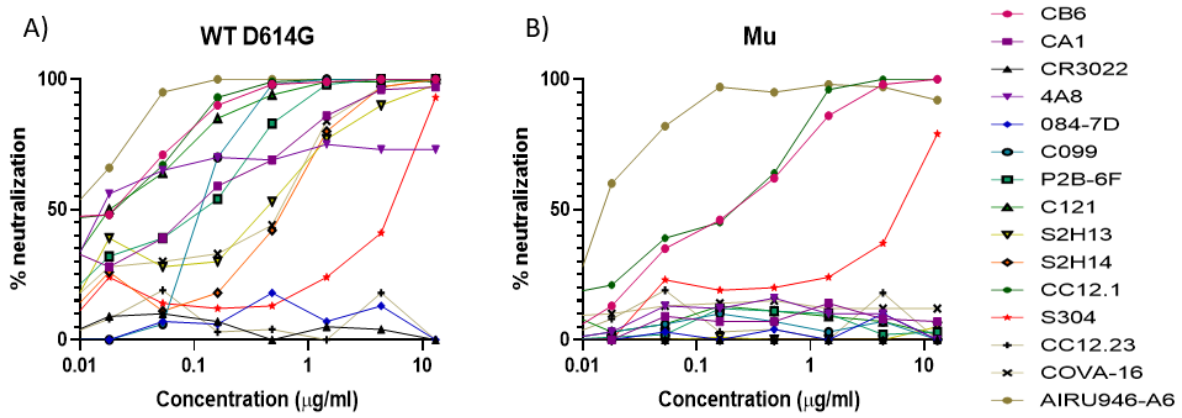

Figure 3. 4 Graphs showing the neutralization of WT D614G and Mu by SARS-CoV-2-specific monoclonal antibodies. WT D614G (A) and Mu (B) were tested against 15 mAbs to determine their cross-reactivity using a SARS-CoV-2 pseudovirus neutralization assay. All samples were tested in duplicate. Vertical (Y) axis shows percentage inhibition and horizontal (X) axis shows antibody concentration in µg/ml.

We found that the neutralizing ability of 13 mAbs against Mu pseudoviruses was significantly decreased when compared with the WT D614G, with the exception of AIRU946-A6 mAb which retained the same level of neutralization against both variants **(Figure 3.4)**. AIRU946-A6 was isolated from a convalescent donor with a Delta break-through infection after receiving the Ad26.COV2.S vaccine, and shows high potency against multiple variants (Kitchin, Bhiman, Moore *et al*, unpublished data).

Mu was neutralized by only four antibodies with different potencies **(Figure 3.4)**. We found that Mu was the most sensitive to neutralization by AIRU946-A6 (IC_{50} = 0.01 µg/mL), followed by CB6 and CC12.1 with IC_{50} values of 0.21 and 0.43 µg/mL, respectively. The CB6 mAb hinders attachment of RBD to the ACE-2 receptor and contends with interface residues (Shi *et al.*, 2020). CC12.1 targets the RBD class 1 epitope of SARS-CoV-2 was identified using high- throughput rapid system from B cells (Rogers et al., 2020). We observed moderate

neutralization of Mu by S304 with an IC_{50} of 6.07 µg/mL. Starr *et al* shows that S304 is able to weakly neutralize Mu which is concordant with our findings.

CR3022, which was isolated from a SARS-CoV-1 convalescent donor, showed no neutralization against both WT D614G and Mu. This is consistent with the published data that shows CR3022 exhibits a high binding affinity to SARS-CoV-2 but no neutralizing capacity (Tian *et al*., 2020; Yuan *et al*., 2020). Gene usage was diverse in the antibodies tested and the majority of the mAbs recognized the RBD. Of the three class I mAbs tested, only one showed complete neutralization escape. Two of the class one antibodies shared the same gene usage (IGHV1-18) but displayed different neutralization profiles towards Mu **(Figure 3.5)**. This may suggest that gene usage does not correlate with antibody potency or breadth. None of the class 2 and 4 mAbs exhibited neutralizing activity towards Mu. The NTD targeting 4A8 mAb exhibited potent neutralizing ability against WT D614G but showed complete loss of neutralization of Mu **(Figure 3.5)**. Overall, there was complete loss in neutralization of Mu by most mAbs compared to WT D614G.

mAbs				Viruses		Fold
Name	Antibody Class	Targeted Epitope	IGH Gene usage	WT D614G	Mu	Change
4A8	N/A	NTD	IGHV1-24	0,01	10	K.O
CB6	Class 1	RBD	IGHV1-18	0,01	0,21	21
CA1	Class 1	RBD	IGHV1-18	0,09	10	K.O
084-7D	Unknown	RBD	IGHV1-3-23*01	10	10	K.O
CR3022	Class 4	RBD	IGHV5-51	10	10	K.O
C099	Class 3	RBD	IGHV3-53	0,11	10	K.O
COVA-16	Class 3	RBD	IGHV1-46	0,56	10	K.O
CC12,23	Unknown	RBD	IGHV4-39	10	10	1
P2B 2F6	Class 2	RBD	IGHV4-38*2	0,12	10	K.O
C121	Class 2	RBD	IGHV1-24	0,01	10	K.O
S2H13	Class 2	RBD	IGHV3-7	0,41	10	K.O
S2H14	Class 1	RBD	IGHV3-15	1,2	10	K.O
CC12,1	Class 1	RBD	IGHV3-53	0,02	0,43	22
S304	Class 3/4	RBD	IGHV1-37	5,23	6,07	1
AIRU946-A6	Unknown	RBD	IGHV1-69	0,01	0,01	1

Fold Change
<5
>5
K.O

Figure 3. 5 Summary of IC50 values showing neutralization of WT D614G and Mu by monoclonal antibodies. The warmer the colour, the more potent the neutralization of the virus by the mAb. Red denotes IC50 values below 0.1 µg/ml, orange denotes values between 0.01 µg/ml and 1 µg/ml, l, yellow for values between 1 µg/ml and 10 µg/ml, and blue for more than 10 µg/ml (which represents neutralization resistance). Fold changes relative to the WT D614G variant are shown. Complete neutralization knock out is signified in black, dark grey signifies fold adjustments of >5 and <5 denoted by light grey.

3.4 The Mu variant shows neutralization escape from antibodies triggered by the WT D614G and Delta variants

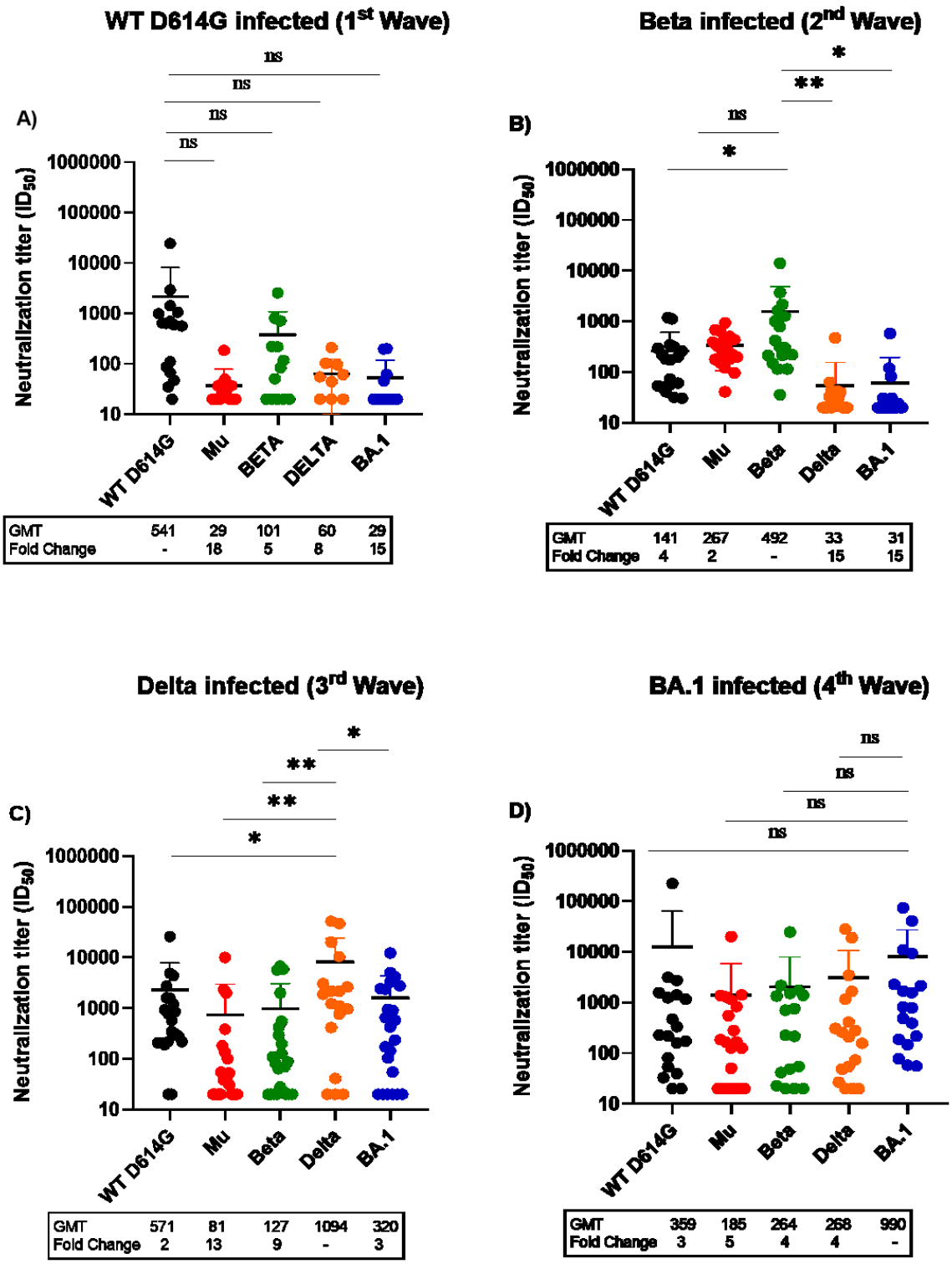

Figure 3. 6 Neutralization titer (ID50) in convalescent plasma from participants infected with (A) WT D614G, (B) Beta, (C) Delta and (D) BA. Plasma was tested against the infecting variant and Mu. Geometric mean titers (GMT) also denoted beneath the plot, Fold change relative to the infecting strain is also shown below the plot. Neutralization titer is shown as an ID_{50} (reciprocal of the serum dilution required to reduce 50% of the virus) Statistical significance was determined using the Friedman test with Dunn's correction. *p<0.05; **p<0.01; ***p<0.001; ****p<0.0001 and ns = non-significant.

We next used a pseudovirus neutralization assay to assess the ability of plasma from convalescent donors infected with either the WT D614G, Beta, Delta or Omicron (BA.1) variants to cross-neutralize other variants. We evaluated plasma from infection with WT D614G strain against other variants. The accumulation of mutations by these variants has resulted in loss of neutralization with fold changes in GMT's ranging from 5 to 18. However, WT D614G retained high autologous neutralization with a GMT of 541 **(Figure 3.6A**). Plasma from infection with Beta was highly cross-reactive against Mu and D614G variant (2-4 fold loss) but was less cross-reactive to Delta and BA.1 with average fold loss of 15 against both variants and a GMT of 31 and 33, respectively (**Figure 3.6B**).

Infection with the Delta variant elicited the highest autologous neutralization with GMT of 1094 (**Figure 3.6C**). Delta plasma also had cross-neutralizing antibodies against WT D614G and BA.1 with neutralization GMT fold losses of 2 and 3, however there was poor cross-reactivity to both Beta and Mu with GMT of 127 and 81 respectively (9-13 fold reduction) (**Figure 3.6C**). Our data confirms many studies showing the capacity of Beta to escape neutralization stimulated by Delta infection (Cele *et al.*, 2021; Bekliz *et al.*, 2022; Moyo-Gwete *et al.*, 2022). Infection with Omicron BA.1 triggered good cross-neutralizing responses with minimal fold loss in GMT's ranging from 5 to 3 (**Figure 3.6D**). Overall, all plasma had good neutralizing responses against the infecting, autologous variant.

A spider plot was generated using neutralization response geometric mean titres to visualise the level of cross-reactive neutralizing antibodies induced by infection with WT D614G, Beta, Delta and BA.1 towards the Mu variant. There was pronounced loss of neutralization of Mu from antibodies elicited by infection with WT D61G with a GMT of 29 **(Figure 3.7)**.

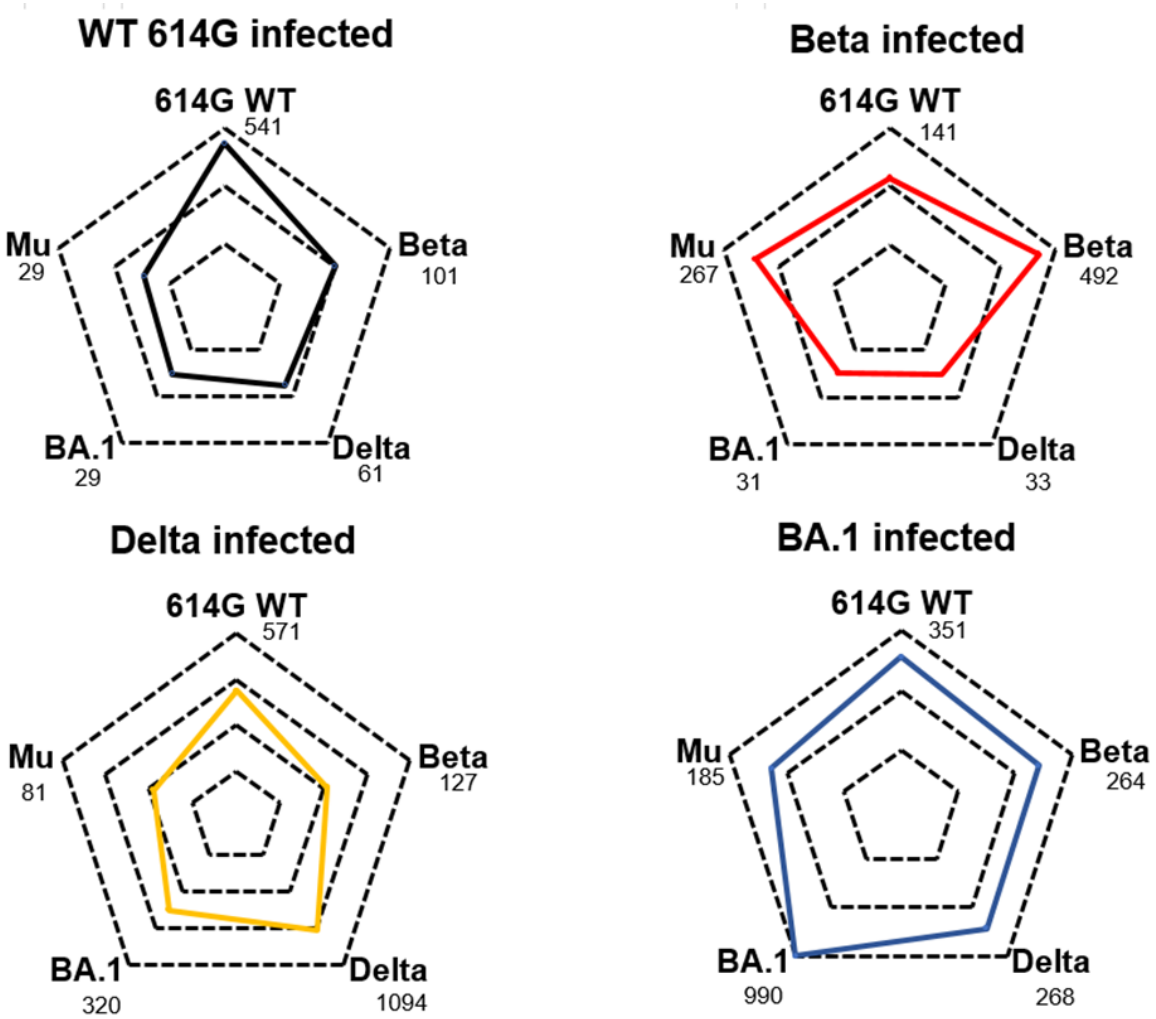

Figure 3. 7 Spider plot of the neutralization geometric mean titer of each variant. Coloured lines closer to the centre or origin of the plot signifies low levels of cross-reactivity while lines close to the perimeter signifies broad cross-reactivity.

Antibodies elicited by the Beta variant exhibited higher levels of cross-reactivity towards the Mu variant (GMT: 267) when compared to those elicited by other variants and this was followed by plasma from infection with BA.1 with a GMT of 186 **(Figure 3.7)**. WT D614G plasma was the least cross-reactive to Mu with a GMT of 29 followed by plasma from infection with Delta variant with a GMT of 81. Overall infection with BA.1 triggered the most cross-reactive antibodies against all VOCs tested, followed by Delta and Beta while D614G was the least broad.

3.5 Determining targets of neutralizing antibody responses to Mu

3.5.1 Confirmation of the functionality of chimeric viruses

Next, we generated chimeric pseudoviruses to determine the target of Mu specific antibody responses using neutralization assays. Site-directed mutagenesis was performed using the SARS-CoV-1 spike as backbone to introduce SARS-CoV-2 Mu RBD and NTD mutations. Antibody resonses towards SARS-CoV-1 are not expected as it has not circulated in the human population since 2003 and it has been previously reported that there is low cross-reactivity between plasma elicited by SARS-CoV-2 infection and SARS-CoV-1. The resulting plasmids were sequenced to confirm that there was successful introduction of the desired mutations (**Supplementary FigureA & B**). This was used to produce pseudoviruses to further explore the specificities of the cross-neutralizing antibodies. The pseudoviruses were tested for entry capacity using ACE-2 cells to confirm the functionality of each of the mutated psuedoviruses (**Table 3.1**). Head to head transfections of all the pseudovirus chimeras were performed to eliminate batch to batch differences in transfection efficiency and cell viability.

Comparison of the wild type viruses, SARS-CoV-1 MU RBD and SARS-CoV-1 MU NTD chimeric pseudoviruses showed that the introduction of SARS-CoV-2 Mu RBD and NTD into the SARS-CoV-1 spike lead to a large reduction in viral entry efficacy with a maximum infectivity of 17 309 RLUs compared to the wild type SARS-CoV-1 value of 533 412 RLUs and the wild type SARS-CoV-2 Mu value of 87 204 RLUs **(Table 3.1)**. This confirmed that the generated pseudovirus chimeras were functional and capable of mediating viral entry into ACE-2 cells, though at a much reduced level compared to either of the parental constructs.

Table 3. 1 Confirmation of the entry capacity of SARS-CoV-1 and SARS-CoV-2 chimeric

Virus Name	Maximum Infectivity (Relative Light Units)
Mu	87 204
SARS-CoV-1	533 412
SARS-CoV-2 Mu RBD	17 309
SARS-CoV-2 Mu NTD	22 016

3.5.2 Delineating epitopes targeted by antibody responses

As we observed the elicitation of cross-reactive antibody responses by other variants against Mu, we next aimed to determine the regions targeted by these cross-reactive antibodies using the chimeric pseudoviruses we generated. A subset of plasma samples with high titres towards Mu were selected for mapping. SARS-CoV-1 was tested as a control to ensure that the responses observed were only towards SARS-CoV-2. Some samples exhibited neutralizing responses towards the SARS-CoV-1 Mu RBD chimera and some wave 2 and wave 4 samples exhibited responses towards both SARS-CoV-1 Mu NTD and SARS-CoV-1 Mu RBD **(Figure 3.8)**. Neutralization of the chimeras was much lower than that of WT Mu, suggesting that the residual responses may be directed towards regions outside of the NTD and RBD. However, unexpectedly, there were responses towards SARS-CoV-1 in some of the samples. In most cases where we saw activity towards the chimeras, we also saw non-specific SARS-CoV-1 neutralizing activity. The high SARS-CoV-1 background means that our results are inconclusive. Positive control antibodies known to neutralize SARS-CoV-2 Mu (AIRU946-A6, CB6, CC12.1 and S304) or SARS-CoV-1 (CR3022 and S304) were used in neutralization assays **(Figure 3.8)**. CR3022 neutralized SARS-CoV-1 Mu RBD chimera which was also unexpected as this is a RBD-directed antibody which cannot neutralize the Mu WT virus. This further suggests that the chimeras were not in the correct conformation. We found that S304 inhibited Mu and both SARS-CoV-1 Mu chimeras viruses less efficiently with the exception of SARS-CoV-1(IC_{50}: 0.19µg/mL) **(Figure 3.8)**.

Infecting strain	Mu	SARS1 MU RBD	SARS1 MU NTD	SARS1
Wave 1 D614G	40	20	20	20
	3535	6638	7611	2259
	29	20	20	20
	186	20	20	20
	37	20	20	20
Wave 2 Beta	461	24	20	20
	651	20	20	20
	686	20	20	20
	507	20	20	20
	336	20	20	20
	940	44	45	20
Wave 3 Delta	136	20	20	20
	100	20	20	20
	384	20	20	20
	1007	32	20	20
	1987	20	20	20
	2342	20	20	20
Wave 4 BA.1	1158	48	374	53
	1399	20	20	20
	1308	240	390	40
	555	70	80	42
	1415	454	416	313
	20187	20	20	135
	165	20	20	20
Control mAbs				
CC12,1	0,14	>13	>13	>13
S304	7,18	6,79	5,31	0,19
CB6	0,25	>13	>13	>13
A6	0,01	>13	>13	>13
CR3022	>13	8,12	2,53	1,26

Figure 3. 8 Summary of neutralization of Mu, SARS-CoV-1 and Chimeras by plasma antibodies. The warmer the colour of the cell, the more potent the neutralization. Red indicates titres that are above 1000. Orange is for dilution factor values between 101 and 1000, yellow for values between 21 and 100, and blue for less than 20 which represents neutralization resistance. The controls at the bottom of the table represents IC_{50} titres and are coloured according to titre where blue represents the inability to neutralize the virus, yellow titres between 1 – 10µg/mL, orange between 0.1 – 0.9µg/mL, and red between 0.01 – 0.09µg/mL.

3.6 Spike recognition at the surface of infected HEK293T cells as targets for ADCC

Fc-mediated effector functions such as ADCC require recognition of the antigen at the surface of the infected cells. However, each transfection could result in varying expression levels of spike. Therefore, flow cytometry was used to validate that there was consistent expression of spike on the surface of HEK293T cells transfected with plasmids expressing WT D614G and Mu variants. The binding of spike-specific mAbs confirmed that there was expression of spike but lack of binding to palivizumab, the negative control, on the surface of HEK293T cells **(Figure 3.9)**.

3.6.1 Spike expression gating strategy and data analysis

HEK293T single cells were gated by size using the forward scatter height vs forward scatter area. In **Figure 3.9,** panel A shows the cell population while panel B shows the gate to eliminate doublets and viability of the population. A histogram was used to represent the spike binding by SARS-CoV-2 specific mAbs as detected by IgG-Alexa fluor 647 florescence (**Figure 3.9C**).

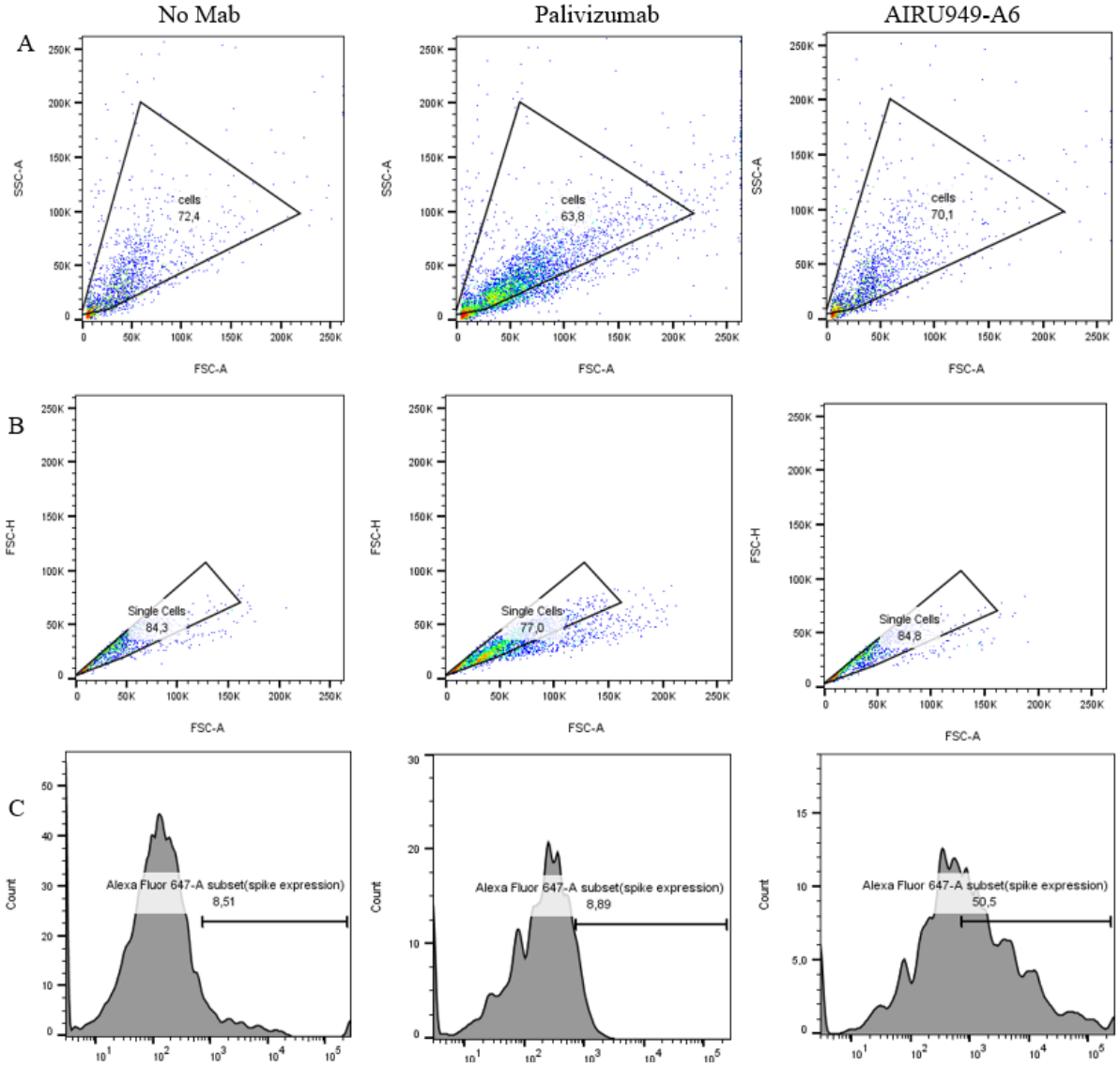

Figure 3. 9 The gating strategy used to analyse spike expression assay in FlowJo™ 10 Software. Each column shows the gating strategy for a different control Row A shows the gating to isolate cells (SSC-A – Side Scatter Area; FSC-A – Forward Scatter Area). Row B shows the gating to select single cells (SSC-H – Side Scatter Height). And row C shows a histogram to gate on cells confirming spike binding using Alexa Flour 647A chanel. No mAb and Palivizumab were used as negative controls. AIRU946-A6 was used as a positive control.

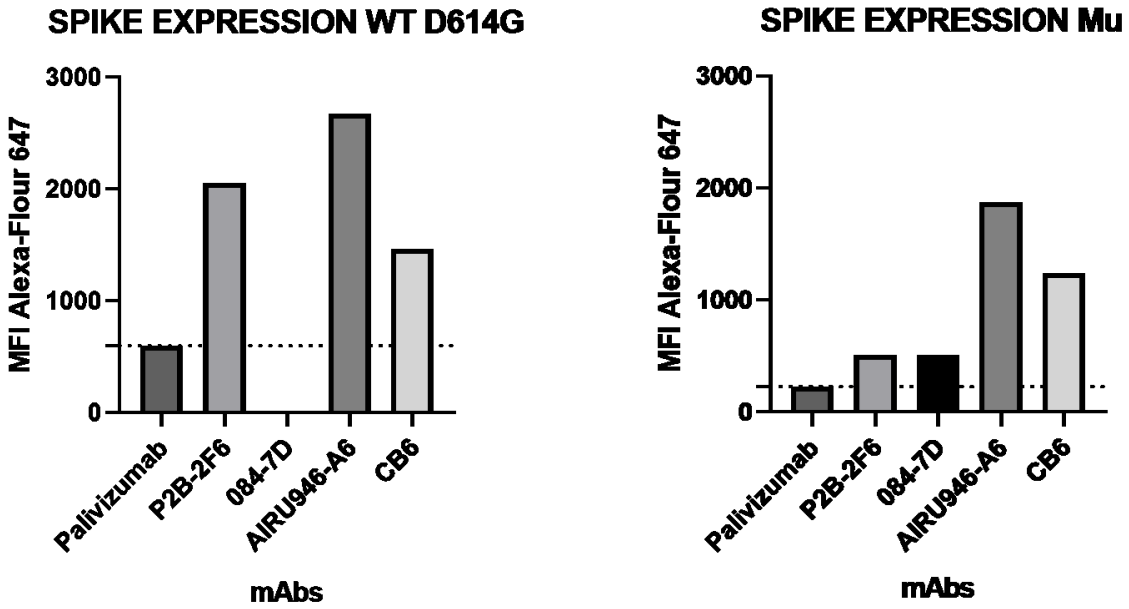

Figure 3. 10 Spike expression on the surface of HEK293T cells transfected with the plasmids expressing WT D614G and Mu spike was measured using flow cytometry 72 hours post-transfection. Spike expression was measured by the mean fluorescent intensity of antibody binding at a concentration of 100 µg/mL followed by staining with an anti-human Fc antibody conjugated to APC (Jackson Labs, 109-135-098) at a 1:100 dilution.

The binding of spike-specific mAbs confirmed that there was expression of spike (for example AIRU-946) but lack of binding to palivizumab, the negative control, on the surface of HEK293T cells (**Figure 3.9C**) as indicated by the shift to the right of fluorescence.

CB6 and AIRU946-A6 strongly bound to both WT D614G and Mu transfected cells and exhibited a bright fluorescence shift detected by the Alexa Fluor 647-A **(Figure 3.10**). The 084-7D mAb did not bind to WT D614G and showed low level of binding to Mu. These results were as expected as we have previously shown that 084-7D is a Beta specific mAb and does not bind to WT D614G (Moyo-Gwete *et al.*, 2022). The binding activity of P2B-2F6 towards WT D614G was high and there was moderate binding to Mu. There was no detectable fluorescence shift for both Palivizumab and the no mAb control wells against both variants **(Figure 3.9C & 3.10)**. Palivizumab did not exhibit any binding as this is a Respiratory Syncytial Virus specific mAb (Romero, 2003). These data confirm that there was adequate spike expression on the surface of HEK239T cells for both variants.

3.7 Antibody Dependent Cellular Cytotoxicity (ADCC) activity is preserved against Mu variant

Next we evaluated the capacity of convalescent plasma to cross-link and activate the FcγRIIIa (CD16) receptor in the presence of Mu spike expressing cells, as a proxy for ADCC. All variants triggered cross-reactive cytotoxic antibodies against Mu. However, the extent of cross-reactivity varied between variants (**Figure 3.11**). Beta and Omicron infection retained significantly higher ADCC activity against Mu with fold losses of 1.6 and 1.5 respectively (**Figure 3.11B & 3.11D**). WT D614G showed a high level of ADCC activity towards Mu with a geometric mean of 312, however it displayed the highest fold loss in ADCC activity with a fold loss of 2.9 when compared to the autologous strain (**Figure 3.11A**).

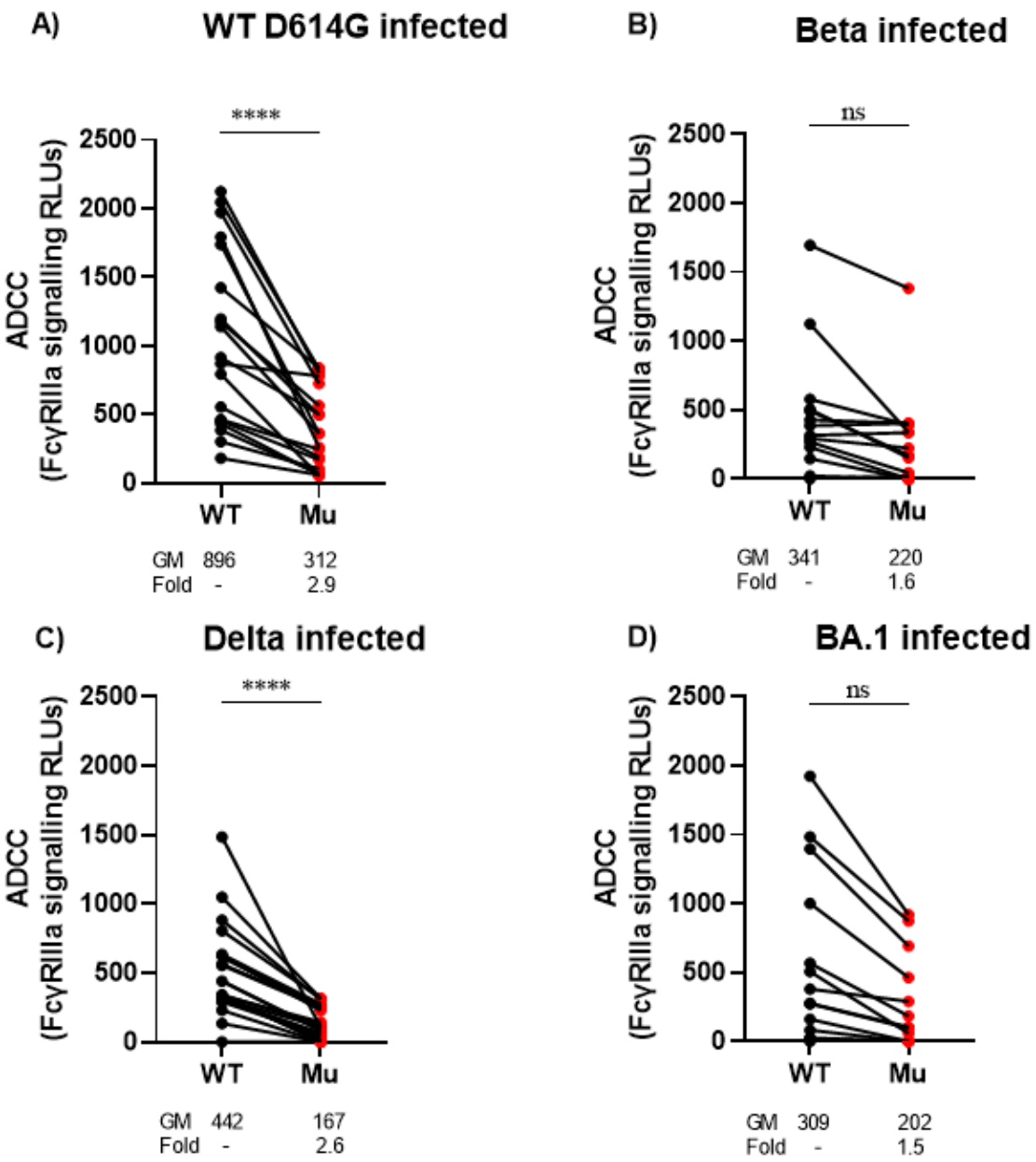

Figure 3. 11 Antibody dependent cellular cytotoxicity (ADCC) with cross-reactivity towards Mu. ADCC is shown as the relative light units (RLU) signalling through C16 activation. WT D614G responses are shown in black while Mu is shown in Red. Statistical significance between variants is calculated using Wilcoxon paired t test; *p < 0.05; **p < 0.01; ***p < 0.001; ****p < 0.0001; and ns = non-significant.

Beta, Delta and BA.1 also triggered cross-reactive cytotoxic antibodies to WT D614G with Delta having the highest heterologous cytotoxic activity to WT D614G with GM of 442, followed by Beta with GM of 341 and lastly BA.1 with GM of 309. Delta infection also showed a substantial loss of ADCC activity towards Mu with a fold loss of 2.6 and GM of 167 (**Figure**

3.11C). Although ADCC against Mu is reduced, it is preserved in convalescent plasma irrespective of the infecting variant. Despite fold losses of activity, there was no variant that displayed complete loss of ADCC activity towards Mu.

4. Discussion

To date, antibody responses targeting the Mu variant have been poorly characterised. In this study, we observed that there was differential targeting of Mu by antibodies elicited by four variants (WT D614G, Beta, Delta and BA.1). We show that regardless of the infecting variant, binding and ADCC responses are mostly preserved towards Mu, but observed varying neutralization escape against Mu. Neutralizing antibodies elicited by the Beta variant exhibited higher levels of cross-reactivity towards Mu while infection with BA.1 triggered moderately cross-reactive antibodies. Convalescent donors infected with WT D614G or Delta showed dramatically reduced cross-reactivity. We observed the same pattern of cross reactive responses against all antibody functions tested when using samples infected with Beta or BA.1 variant indicating that there may be correlations between binding, ADCC, and neutralization responses for these particular groups.

The rise of viral variants that are antigenically distinct from each other has highlighted the importance of continuous monitoring of viral sequences which is crucial to support further vaccine adaptations (Harvey *et al.*, 2021; Rayati Damavandi *et al.*, 2022). Antibody escape mutations pose a threat of re-infections or break-through infections following vaccination and have resulted in a search for improved vaccines that target conserved regions of the spike protein between variants (Haque and Pant, 2022). The potential of another coronavirus or sarbecovirus crossover to humans has also prompted the need to update current vaccines to a cross-clade or a pan-coronavirus vaccine that is able to induce protection against all four major lineages of coronavirus (Li *et al.*, 2021).

Another challenge with existing approved COVID-19 vaccines is that the high levels of protective antibodies induced wane over time. Several studies have shown that bivalent vaccines or heterologous boosting are not only effective at inducing strain specific responses but offer an advantage of eliciting cross-neutralizing antibodies with greater potency and longer durability (Atmar *et al.*, 2021; Collier *et al.*, 2022; Scheaffer *et al.*, 2023). Several companies have now employed a range of technologies and approaches such as the use of ferritin nanoparticles, viral vectors other than adenoviruses, and chimeric spike mRNA encoding antigens from all four human-infecting coronaviruses that cause common colds (Carmen *et al.*, 2021; Joyce *et al.*, 2021; Martinez *et al.*, 2021; Dolgin, 2022; Tai *et al.*, 2022). The need for a

pan-coronavirus vaccine highlights the importance of identifying cross-reactive antibodies and defining their epitopes to provide templates for rational immunogen design.

In this study, all variants elicited cross-reactive binding antibodies although the magnitude of binding to Mu was reduced. Overall, infection with Beta triggered the most cross-reactive binding antibodies against Mu, followed by BA.1 while D614G and Delta were the least cross-reactive. Multiple studies have shown that binding antibody activity is retained against VOCs (Dupont *et al.*, 2021; Richardson *et al.*, 2022). These data suggest that cross-reactivity in antibody binding to the spike protein is common as multiple epitopes on the spike are targeted and this remains the same for the binding responses towards Mu as shown in this study. Slight decreases in binding activity may be a result of mutations in Mu that cause loss of binding epitope recognition. Further work mapping the binding responses may provide insights into the impact of Mu lineage-defining single mutations on binding, however functional studies are likely more informative, as with the assays carried out in this study.

This study highlighted that autologous neutralization was usually higher than heterologous neutralization for all variants tested, which is in line with other research (Liu *et al.*, 2021; Rössler *et al.*, 2022). The Delta variant exhibited the highest homologous neutralization activity which could be due to the high viral loads associated with infection by Delta (Luo *et al.*, 2021; King *et al.*, 2022; von Wintersdorff *et al.*, 2022). Cross-reactive neutralizing responses were broadest in individuals infected with BA.1, whereas infection with WT D614G and Delta resulted in narrow specificity responses. This is in contrast to Straten *et al* and Richardson *et al* where they show that BA.1 developed weak neutralizing responses against the VOCs tested, including the autologous strain (Richardson *et al.*, 2022; van der Straten *et al.*, 2022). The differences in cross-reactivity patterns exhibited by BA.1 could be due to the use of a hospitalised cohort with greater disease severity in our studies, which has been shown to elicit higher antibody responses, and may impact cross-reactivity (Chen *et al.*, 2020; Garcia-Beltran *et al.*, 2021). In the study by Richardson *et al*, despite the use of a hospitalised cohort, most cases were mild as they were only diagnosed after admission, in contrast to the cohort in this study. In addition, although clinical folders were consulted for any prior infections before their BA.1 infection, we cannot rule out asymptomatic infection which may have an impact on antibody responses observed. Several studies have shown that reinfection has a boosting effect

on antibody responses (Cohen and Burbelo, 2020; Edridge *et al.*, 2020). Cross-reactivity in most variants is accounted for by sequence homogeneity between variants (Jette *et al.*, 2021; Li *et al.*, 2022). From the panel of variants tested, Omicron is the most mutated variant which is characterised by 39 mutations with 5 shared mutations between Delta and 4 shared mutations with Beta (Ou *et al.*, 2022; Viana *et al.*, 2022). Therefore, these data suggest that severe infection with the highly mutated Omicron variant induces broad cross-reactive antibodies. Overall the pattern of cross-reactivity varied per variant.

Although Mu was reported as a highly resistant VOI, the antibody resistance profile of Mu remained to be defined. We determined neutralizing cross-reactivity elicited by four distinct SARS-CoV-2 variants towards the Mu variant. Beta and Omicron infection elicited neutralizing responses that were more cross-reactive towards Mu while WT D614G and Delta were the least cross-reactive to Mu. Our results are in line with two studies, which also showed that Mu escaped neutralization from antibodies elicited by infection with WT D614G (Uriu *et al.*, 2021; Tada *et al.*, 2022). Neutralization escape of Mu from antibodies elicited by WT D614G and Delta may be as a result of the 95I mutation located in the NTD, which is known to confer resistance in other variants (McCallum *et al.*, 2021), however this requires confirmatory mutagenesis studies. The resistance of Mu by antibodies elicited by WT D614G or Delta infection may indicate a high risk of re-infection. This mutation may also account for the inability of the NTD-directed 4A8 mAb to neutralize Mu.

Antigenic relationships among the VOCs studied using neutralization data suggests a high degree of antigenic similarity between WT D614G and Delta (van der Straten *et al.*, 2022). This may explain the similar antibody escape patterns observed by these two variants towards Mu. The presence of the RBD R346K and E484K mutations in Mu may further reduce neutralizing activity of antibodies elicited by WT D614G infection as they are associated with neutralization escape by class I and II antibodies (Greaney *et al.*, 2021; Wibmer *et al.*, 2021). This is consistent with our findings as all class II antibodies tested had complete neutralization escape from Mu. Beta and Omicron share key antibody escape site mutations with the Mu variant, which may account for the exhibited level of cross-reactivity by these two variants. An antigenic map by Mykytyn *et al* reveals that Beta, Gamma and Mu variants all cluster close to each other and this may account for high levels of cross-reactivity towards Mu variant by

antibodies elicited by infection with Beta (Mykytyn *et al.*, 2022). BA.1 shows moderate levels of cross-reactivity towards Mu compared to Beta and has been found to be antigenically distinct from all other variants (Wang *et al.*, 2022). Future studies using absorbed BA.1 plasma may reveal epitopes targeted towards Mu by these responses. One limitation of our study is lack of convalescent plasma from individuals infected with the Mu variant to determine the changes in binding and neutralization sensitivity of the VOCs tested relative to Mu-elicited plasma.

Epitope-directed mutagenesis was intended to identify key mutations that mediate neutralization escape in Mu. However, this was not achieved as the pseudovirus produced was not optimal. Neutralization of the engineered chimeras was observed only in antibodies that recognize SARS-CoV-1, suggesting that the spike was folded incorrectly. The introduction of SARS-CoV-2 Mu RBD and NTD into SARS-CoV-1 spike led to a significant reduction in viral entry. Although Sanger sequencing confirmed the correct incorporation of mutations, all SARS-CoV-2 specific mAbs failed to neutralize the chimeric virus, this may suggest that the structure of the virus was altered on the ACE2 receptor binding site in a manner that resulted in reducing virus-host interactions. This interpretation will require further investigation by structural studies such as transmission electron microscopy (TEM) which is an imaging technique that allows direct visualisation of whole viruses.. Future studies could identify the viral epitopes targeted by neutralizing antibodies by using plasma adsorption methods which have been successfully used in HIV-1 infection (Gray *et al.*, 2009; Wibmer *et al.*, 2013).

Several studies highlight that ADCC plays a critical role in clearing infection and is associated with vaccine protection against SARS-CoV-2 (Dufloo *et al.*, 2021; Tso *et al.*, 2021). The ADCC response against the Mu variant had not been determined before this study. ADCC responses have been shown to be preserved against VOCs (Richardson *et al.*, 2021; Richardson *et al.*, 2022; Richardson *et al.*, 2022). This study found the same to be true for Mu. However, the level at which ADCC is preserved varies per infecting variant. ADCC responses triggered by Beta and BA.1 were more cross-reactive to Mu than those triggered by WT and Delta. This may suggest that the infecting variant has an effect on the extent of ADCC cross-reactivity (Richardson *et al.*, 2022). Although this analysis was based on heterologous responses against Beta, Delta and BA.1 with the exception of WT D614G, comparing autologous responses should be considered as a next step. Generally, ADCC fold loss in activity ranged between 1

to 3, which is consistent with what others have reported and is far less than the losses seen for neutralization (Kaplonek *et al.*, 2022; Richardson *et al.*, 2022). The preservation of ADCC may be a result of antibodies targeting epitopes or sites beyond those commonly mutated in VOCs, such as the S2 region. This is in line with the observation that RBD and NTD are not the only target of ADCC responses (Kaplonek *et al.*, 2021). Future studies should include mapping of epitopes targeted by Fc effector mediated response, as these may identify important sites to target through vaccination to induce potent and broad Fc responses.

In summary, our data demonstrated that the SARS-CoV-2 Mu variant shows variable escape from humoral responses triggered by four different variants. Our data also confirms that Mu is a resistant VOI as previously reported by others (Uriu *et al.*, 2021, 2022; Tada *et al.*, 2022). The variable escape of Mu by antibodies highlights the need to identify epitopes targeted by neutralization resistant SARS-CoV-2 variants as this may aid in immunogen design strategies for next-generation vaccines.

5. Conclusion

This study aimed to assess whether there was differential targeting of Mu by antibodies elicited by four variants (WT D614G, Beta, Delta and Omicron (BA.1)) responsible for the first four waves of COVID-19 infection in South Africa. We used convalescent plasma to measure binding, neutralization and ADCC activity against Mu, and compared the level of cross-reactivity across each of the waves. The Mu lineage defining mutations mostly occur in the RBD and the NTD, which are the primary targets of neutralizing antibodies. We observed that binding and ADCC responses were mostly preserved towards Mu. However, there was variable neutralization escape. In this study, the Beta variant exhibited higher levels of cross-reactivity towards Mu followed by BA.1 while Delta and WT D614G had the largest fold decrease for neutralization against Mu. This suggests that various functions are affected differently by VOC/VOIs. This may be due to binding and ADCC responses recognizing more epitopes on the spike in regions without VOC/VOI mutations compared to neutralizing antibodies. In this study we also show that the overall pattern of neutralization cross-reactivity varied depending on the infecting variant, indicating that the spike sequence of the infecting variant had an effect on the quality of neutralizing antibodies elicited. Results from this study highlight the importance of continued viral genomic surveillance and studying immune escape of neutralization resistant variants from convalescent sera. This study provides insights into how antibody responses elicited by different VOCs differentially target the Mu variant spike. As Mu shares multiple mutations with other VOCS, this data will expand current knowledge on the effects of SARS-CoV-2 spike mutations and may help us predict the impact of mutations that may be common to emerging VOCs. These data may also provide insights on next generation vaccine design based on neutralization-resistant SARS-COV-2 variants.

6. References

Ackerman, M.E. *et al.* (2013) 'Enhanced Phagocytic Activity of HIV-Specific Antibodies Correlates with Natural Production of Immunoglobulins with Skewed Affinity for FcγR2a and FcγR2b', *Journal of Virology*, 87(10), pp. 5468–5476. Available at: https://doi.org/10.1128/JVI.03403-12.

Alberts, B. *et al.* (2002) 'B Cells and Antibodies', *Molecular Biology of the Cell. 4th edition*. Available at: https://www.ncbi.nlm.nih.gov/books/NBK26884/ (Accessed: 15 February 2023).

Alter, G. *et al.* (2021) 'Immunogenicity of Ad26.COV2.S vaccine against SARS-CoV-2 variants in humans', *Nature*, 596(7871), pp. 268–272. Available at: https://doi.org/10.1038/S41586-021-03681-2.

Atmar, R.L. *et al.* (2021) 'Heterologous SARS-CoV-2 Booster Vaccinations – Preliminary Report', *medRxiv*, p. 2021.10.10.21264827. Available at: https://doi.org/10.1101/2021.10.10.21264827.

Baden, L.R. *et al.* (2020) 'Efficacy and Safety of the mRNA-1273 SARS-CoV-2 Vaccine', *https://doi.org/10.1056/NEJMoa2035389*, 384(5), pp. 403–416. Available at: https://doi.org/10.1056/NEJMOA2035389.

Barnes, C.O. *et al.* (2020) 'SARS-CoV-2 neutralizing antibody structures inform therapeutic strategies', *Nature*, 588(7839), pp. 682–687. Available at: https://doi.org/10.1038/s41586-020-2852-1.

Bekliz, M. *et al.* (2022) 'Neutralization capacity of antibodies elicited through homologous or heterologous infection or vaccination against SARS-CoV-2 VOCs', *Nature Communications*, 13(1), p. 3840. Available at: https://doi.org/10.1038/s41467-022-31556-1.

Boehm, E. *et al.* (2021) 'Novel SARS-CoV-2 variants: the pandemics within the pandemic', *Clinical Microbiology and Infection* [Preprint]. Available at: https://doi.org/10.1016/j.cmi.2021.05.022.

Brobst, B. and Borger, J. (2022) 'Benefits And Risks Of Administering Monoclonal Antibody Therapy For Coronavirus (COVID-19)', *StatPearls* [Preprint]. Available at:

https://www.ncbi.nlm.nih.gov/books/NBK574507/ (Accessed: 14 November 2022).

Bruxvoort, K.J. *et al.* (2021) 'Effectiveness of mRNA-1273 against delta, mu, and other emerging variants of SARS-CoV-2: test negative case-control study', *BMJ*, 375. Available at: https://doi.org/10.1136/BMJ-2021-068848.

Burton, D.R. and Topol, E.J. (2021) 'Variant-proof vaccines - invest now for the next pandemic', *Nature*, 590(7846), pp. 386–388. Available at: https://doi.org/10.1038/D41586-021-00340-4.

Carmen, J.M. *et al.* (2021) 'SARS-CoV-2 ferritin nanoparticle vaccine induces robust innate immune activity driving polyfunctional spike-specific T cell responses', *npj Vaccines*, 6(1), pp. 1–18. Available at: https://doi.org/10.1038/s41541-021-00414-4.

Cele, S. *et al.* (2021) 'SARS-CoV-2 evolved during advanced HIV disease immunosuppression has Beta-like escape of vaccine and Delta infection elicited immunity', *medRxiv: The Preprint Server for Health Sciences*, p. 2021.09.14.21263564. Available at: https://doi.org/10.1101/2021.09.14.21263564.

Cevik, M. *et al.* (2020) 'Virology, transmission, and pathogenesis of SARS-CoV-2', *The BMJ*, 371. Available at: https://doi.org/10.1136/bmj.m3862.

Chan, C.E.Z. *et al.* (2021) 'The Fc-mediated effector functions of a potent SARS-CoV-2 neutralizing antibody, SC31, isolated from an early convalescent COVID-19 patient, are essential for the optimal therapeutic efficacy of the antibody', *PLOS ONE*, 16(6), p. e0253487. Available at: https://doi.org/10.1371/JOURNAL.PONE.0253487.

Chen, X. *et al.* (2020) 'Disease severity dictates SARS-CoV-2-specific neutralizing antibody responses in COVID-19', *Signal Transduction and Targeted Therapy*, 5(1), pp. 1–6. Available at: https://doi.org/10.1038/s41392-020-00301-9.

Chi, X. *et al.* (2020) 'A neutralizing human antibody binds to the N-terminal domain of the Spike protein of SARS-CoV-2', *Science*, 369(6504), pp. 650–655. Available at: https://doi.org/10.1126/SCIENCE.ABC6952.

Chiu, M.L. *et al.* (2019) 'Antibody Structure and Function: The Basis for Engineering

Therapeutics', *Antibodies*, 8(4), p. 55. Available at: https://doi.org/10.3390/antib8040055.

Cohen, J.I. and Burbelo, P.D. (2020) 'Reinfection With SARS-CoV-2: Implications for Vaccines', *Clinical Infectious Diseases: An Official Publication of the Infectious Diseases Society of America*, 73(11), pp. e4223–e4228. Available at: https://doi.org/10.1093/cid/ciaa1866.

Collier, A.Y. *et al.* (2022) 'Immunogenicity of the BA.5 Bivalent mRNA Vaccine Boosters'. bioRxiv, p. 2022.10.24.513619. Available at: https://doi.org/10.1101/2022.10.24.513619.

Corbett, K.S. *et al.* (2020) 'Evaluation of the mRNA-1273 Vaccine against SARS-CoV-2 in Nonhuman Primates', *https://doi.org/10.1056/NEJMoa2024671*, 383(16), pp. 1544–1555. Available at: https://doi.org/10.1056/NEJMOA2024671.

Corti, D. *et al.* (2021) 'Tackling COVID-19 with neutralizing monoclonal antibodies', *Cell*, 184(12), pp. 3086–3108. Available at: https://doi.org/10.1016/j.cell.2021.05.005.

Dai, L. and Gao, G.F. (2021) 'Viral targets for vaccines against COVID-19', *Nature Reviews Immunology*, 21(2), pp. 73–82. Available at: https://doi.org/10.1038/s41577-020-00480-0.

Dolgin, E. (2022) 'Pan-coronavirus vaccine pipeline takes form', *Nature Reviews Drug Discovery*, 21(5), pp. 324–326. Available at: https://doi.org/10.1038/D41573-022-00074-6.

Dufloo, J. *et al.* (2021) 'Asymptomatic and symptomatic SARS-CoV-2 infections elicit polyfunctional antibodies', *Cell reports. Medicine*, 2(5). Available at: https://doi.org/10.1016/J.XCRM.2021.100275.

Dupont, L. *et al.* (2021) 'Neutralizing antibody activity in convalescent sera from infection in humans with SARS-CoV-2 and variants of concern', *Nature Microbiology*, 6(11), pp. 1433–1442. Available at: https://doi.org/10.1038/s41564-021-00974-0.

Edridge, A.W.D. *et al.* (2020) 'Seasonal coronavirus protective immunity is short-lasting', *Nature Medicine*, 26(11), pp. 1691–1693. Available at: https://doi.org/10.1038/s41591-020-1083-1.

Elsaghir, H. and Adnan, G. (2022) 'Best Practices For Administering Monoclonal Antibody Therapy For Coronavirus (COVID-19)', *StatPearls*. Available at:

https://www.ncbi.nlm.nih.gov/books/NBK572140/ (Accessed: 14 November 2022).

van Erp, E.A. *et al.* (2019) 'Fc-Mediated Antibody Effector Functions During Respiratory Syncytial Virus Infection and Disease', *Frontiers in Immunology*, 10. Available at: https://www.frontiersin.org/articles/10.3389/fimmu.2019.00548 (Accessed: 15 February 2023).

Estes, B. *et al.* (2021) 'Next generation Fc scaffold for multispecific antibodies', *iScience*, 24(12), p. 103447. Available at: https://doi.org/10.1016/j.isci.2021.103447.

Fan, X. *et al.* (2020) 'Cryo-EM analysis of the post-fusion structure of the SARS-CoV spike glycoprotein', *Nature Communications 2020 11:1*, 11(1), pp. 1–10. Available at: https://doi.org/10.1038/s41467-020-17371-6.

Fouladirad, S. and Bach, H. (2021) 'Development of Coronavirus Treatments Using Neutralizing Antibodies', *Microorganisms*, 9(1), p. 165. Available at: https://doi.org/10.3390/microorganisms9010165.

Fratev, F. (2021) 'The R346K Mutation in the Mu Variant of SARS-CoV-2 Alter the Interactions with Monoclonal Antibodies from Class 2: A Free Energy of Perturbation Study', *bioRxiv*, p. 2021.10.12.463781. Available at: https://doi.org/10.1101/2021.10.12.463781.

Garcia-Beltran, W.F. *et al.* (2021) 'COVID-19-neutralizing antibodies predict disease severity and survival', *Cell*, 184(2), pp. 476-488.e11. Available at: https://doi.org/10.1016/j.cell.2020.12.015.

Gorbalenya, A.E., Baker, S.C., Baric, R.S., Groot, R.J. de, *et al.* (2020) 'Severe acute respiratory syndrome-related coronavirus: The species and its viruses – a statement of the Coronavirus Study Group', *bioRxiv*, p. 2020.02.07.937862. Available at: https://doi.org/10.1101/2020.02.07.937862.

Gorbalenya, A.E., Baker, S.C., Baric, R.S., de Groot, R.J., *et al.* (2020) 'The species Severe acute respiratory syndrome-related coronavirus: classifying 2019-nCoV and naming it SARS-CoV-2', *Nature Microbiology*, 5(4), pp. 536–544. Available at: https://doi.org/10.1038/S41564-020-0695-Z.

Gray, E.S. *et al.* (2009) 'Antibody Specificities Associated with Neutralization Breadth in Plasma from Human Immunodeficiency Virus Type 1 Subtype C-Infected Blood Donors', *Journal of Virology*, 83(17), pp. 8925–8937. Available at: https://doi.org/10.1128/JVI.00758-09.

Greaney, A.J. *et al.* (2021) 'Mutational escape from the polyclonal antibody response to SARS-CoV-2 infection is largely shaped by a single class of antibodies.', *bioRxiv : the preprint server for biology* [Preprint]. Available at: https://doi.org/10.1101/2021.03.17.435863.

Gupta, D. *et al.* (2021) 'Structural and functional insights into the spike protein mutations of emerging SARS-CoV-2 variants', *Cellular and Molecular Life Sciences 2021 78:24*, 78(24), pp. 7967–7989. Available at: https://doi.org/10.1007/S00018-021-04008-0.

Haid, S. *et al.* (2016) 'Identification of a Human Respiratory Syncytial Virus Cell Entry Inhibitor by Using a Novel Lentiviral Pseudotype System', *Journal of Virology*, 90(6), pp. 3065–3073. Available at: https://doi.org/10.1128/JVI.03074-15.

Hansen, J. *et al.* (2020) 'Studies in humanized mice and convalescent humans yield a SARS-CoV-2 antibody cocktail', *Science (New York, N.y.)*, 369(6506), p. 1010. Available at: https://doi.org/10.1126/SCIENCE.ABD0827.

Haque, A. and Pant, A.B. (2022) 'Mitigating Covid-19 in the face of emerging virus variants, breakthrough infections and vaccine hesitancy', *Journal of Autoimmunity*, 127, p. 102792. Available at: https://doi.org/10.1016/j.jaut.2021.102792.

Harvey, W.T. *et al.* (2021) 'SARS-CoV-2 variants, spike mutations and immune escape', *Nature Reviews Microbiology 2021 19:7*, 19(7), pp. 409–424. Available at: https://doi.org/10.1038/s41579-021-00573-0.

Janda, A. *et al.* (2016) 'Ig Constant Region Effects on Variable Region Structure and Function', *Frontiers in Microbiology*, 7. Available at: https://www.frontiersin.org/articles/10.3389/fmicb.2016.00022 (Accessed: 15 February 2023).

Jette, C.A. *et al.* (2021) 'Broad cross-reactivity across sarbecoviruses exhibited by a subset of COVID-19 donor-derived neutralizing antibodies'. bioRxiv, p. 2021.04.23.441195. Available at: https://doi.org/10.1101/2021.04.23.441195.

Jin, D., Wei, J. and Sun, J. (2021) 'Analysis of the molecular mechanism of SARS-CoV-2 antibodies', *Biochemical and Biophysical Research Communications*, 566, p. 45. Available at: https://doi.org/10.1016/J.BBRC.2021.06.001.

Joyce, M.G. *et al.* (2021) 'SARS-CoV-2 ferritin nanoparticle vaccines elicit broad SARS coronavirus immunogenicity', *bioRxiv*, p. 2021.05.09.443331. Available at: https://doi.org/10.1101/2021.05.09.443331.

Ju, B. *et al.* (2020) 'Human neutralizing antibodies elicited by SARS-CoV-2 infection', *Nature*, 584(7819), pp. 115–119. Available at: https://doi.org/10.1038/s41586-020-2380-z.

Kaplonek, P. *et al.* (2021) 'Early cross-coronavirus reactive signatures of humoral immunity against COVID-19', *Science Immunology*, 6(64), p. eabj2901. Available at: https://doi.org/10.1126/sciimmunol.abj2901.

Kaplonek, P. *et al.* (2022) 'mRNA-1273 vaccine-induced antibodies maintain Fc effector functions across SARS-CoV-2 variants of concern'. Available at: https://doi.org/10.1016/j.immuni.2022.01.001.

Keeton, R. *et al.* (2021) 'Prior infection with SARS-CoV-2 boosts and broadens Ad26.COV2.S immunogenicity in a variant-dependent manner', *Cell host & microbe*, 29(11), pp. 1611-1619.e5. Available at: https://doi.org/10.1016/J.CHOM.2021.10.003.

Khoury, D.S. *et al.* (2021) 'Neutralizing antibody levels are highly predictive of immune protection from symptomatic SARS-CoV-2 infection', *Nature Medicine*. Available at: https://doi.org/10.1038/S41591-021-01377-8.

King, K.L. *et al.* (2022) 'SARS-CoV-2 variants of concern Alpha and Delta show increased viral load in saliva', *medRxiv*, p. 2022.02.10.22270797. Available at: https://doi.org/10.1101/2022.02.10.22270797.

Kitchin, D. *et al.* (2022) 'Ad26.COV2.S breakthrough infections induce high titers of neutralizing antibodies against Omicron and other SARS-CoV-2 variants of concern', *Cell Reports Medicine*, 3(3), p. 100535. Available at: https://doi.org/10.1016/j.xcrm.2022.100535.

Koff, W.C. and Berkley, S.F. (2021) 'A universal coronavirus vaccine', *Science (New York,*

N.Y.), 371(6531), p. 759. Available at: https://doi.org/10.1126/SCIENCE.ABH0447.

Lee, W.S. *et al.* (2021) 'Decay of Fc-dependent antibody functions after mild to moderate COVID-19', *Cell Reports Medicine*, 2(6), p. 100296. Available at: https://doi.org/10.1016/J.XCRM.2021.100296.

Li, Q. *et al.* (2018) 'Current status on the development of pseudoviruses for enveloped viruses', *Reviews in Medical Virology*, 28(1), p. e1963. Available at: https://doi.org/10.1002/rmv.1963.

Li, Q. *et al.* (2022) 'Cross-reactivity of eight SARS-CoV-2 variants rationally predicts immunogenicity clustering in sarbecoviruses', *Signal Transduction and Targeted Therapy*, 7, p. 256. Available at: https://doi.org/10.1038/s41392-022-01123-7.

Li, X. *et al.* (2021) 'Possible Targets of Pan-Coronavirus Antiviral Strategies for Emerging or Re-Emerging Coronaviruses', *Microorganisms*, 9(7), p. 1479. Available at: https://doi.org/10.3390/microorganisms9071479.

Lim, W.W. and Cowling, B.J. (2022) 'Mechanistic Correlates of Protection for SARS-CoV-2 Vaccines', *Epidemiology*, 33(1), pp. e1–e1. Available at: https://doi.org/10.1097/EDE.0000000000001419.

Liu, C. *et al.* (2021) 'Reduced neutralization of SARS-CoV-2 B.1.617 by vaccine and convalescent serum', *Cell*, 184(16), pp. 4220-4236.e13. Available at: https://doi.org/10.1016/J.CELL.2021.06.020.

Liu, Y. *et al.* (2021) 'Delta spike P681R mutation enhances SARS-CoV-2 fitness over Alpha variant', *bioRxiv*, p. 2021.08.12.456173. Available at: https://doi.org/10.1101/2021.08.12.456173.

Li, C.-J. *et al.* (2022) 'Neutralizing Monoclonal Antibodies Inhibit SARS-CoV-2 Infection through Blocking Membrane Fusion', *Microbiology Spectrum*, 10(2), p. e0181421. Available at: https://doi.org/10.1128/spectrum.01814-21.

Luo, C.H. *et al.* (2021) 'Infection with the SARS-CoV-2 Delta Variant is Associated with Higher Infectious Virus Loads Compared to the Alpha Variant in both Unvaccinated and Vaccinated Individuals', *medRxiv*, p. 2021.08.15.21262077. Available at:

https://doi.org/10.1101/2021.08.15.21262077.

Luo, S. et al. (2022) 'An antibody from single human VH-rearranging mouse neutralizes all SARS-CoV-2 variants through BA.5 by inhibiting membrane fusion', Science Immunology, 7(76), p. eadd5446. Available at: https://doi.org/10.1126/sciimmunol.add5446.

Madhi, S.A. *et al.* (2021) 'Efficacy of the ChAdOx1 nCoV-19 Covid-19 Vaccine against the B.1.351 Variant', *https://doi.org/10.1056/NEJMoa2102214*, 384(20), pp. 1885–1898. Available at: https://doi.org/10.1056/NEJMOA2102214.

Martinez, D.R. *et al.* (2021) 'Chimeric spike mRNA vaccines protect against Sarbecovirus challenge in mice', *bioRxiv*, p. 2021.03.11.434872. Available at: https://doi.org/10.1101/2021.03.11.434872.

McCallum, M., Walls, A.C., *et al.* (2021) 'Molecular basis of immune evasion by the Delta and Kappa SARS-CoV-2 variants.', *Science (New York, N.Y.)*, p. eabl8506. Available at: https://doi.org/10.1126/SCIENCE.ABL8506.

McCallum, M., De Marco, A., *et al.* (2021) 'N-terminal domain antigenic mapping reveals a site of vulnerability for SARS-CoV-2', *Cell*, 184(9), pp. 2332-2347.e16. Available at: https://doi.org/10.1016/j.cell.2021.03.028.

Morens, D.M., Taubenberger, J.K. and Fauci, A.S. (2022) 'Universal Coronavirus Vaccines - An Urgent Need', *The New England journal of medicine*, 386(4), pp. 297–299. Available at: https://doi.org/10.1056/NEJMP2118468.

Moyo-Gwete, T. *et al.* (2021) 'Cross-Reactive Neutralizing Antibody Responses Elicited by SARS-CoV-2 501Y.V2 (B.1.351)', *https://doi.org/10.1056/NEJMc2104192*, 384(22), pp. 2161–2163. Available at: https://doi.org/10.1056/NEJMC2104192.

Moyo-Gwete, T. *et al.* (2022) 'Shared N417-Dependent Epitope on the SARS-CoV-2 Omicron, Beta, and Delta Plus Variants', *Journal of Virology*. Edited by T. Gallagher. Available at: https://doi.org/10.1128/JVI.00558-22.

Mykytyn, A.Z. *et al.* (2022) 'Omicron BA.1 and BA.2 are antigenically distinct SARS-CoV-2 variants'. bioRxiv, p. 2022.02.23.481644. Available at:

https://doi.org/10.1101/2022.02.23.481644.

Neerukonda, S.N. *et al.* (2021) 'Establishment of a well-characterized SARS-CoV-2 lentiviral pseudovirus neutralization assay using 293T cells with stable expression of ACE2 and TMPRSS2', *PLOS ONE*, 16(3), p. e0248348. Available at: https://doi.org/10.1371/journal.pone.0248348.

Ou, J. *et al.* (2022) 'Tracking SARS-CoV-2 Omicron diverse spike gene mutations identifies multiple inter-variant recombination events', *Signal Transduction and Targeted Therapy*, 7(1), pp. 1–9. Available at: https://doi.org/10.1038/s41392-022-00992-2.

Pinto, D. *et al.* (2020) 'Cross-neutralization of SARS-CoV-2 by a human monoclonal SARS-CoV antibody', *Nature*, 583(7815), pp. 290–295. Available at: https://doi.org/10.1038/s41586-020-2349-y.

Plante, J.A. *et al.* (2021) 'The variant gambit: COVID-19's next move', *Cell host & microbe*. Available at: https://doi.org/10.1016/j.chom.2021.02.020.

Polack, F.P. *et al.* (2020) 'Safety and Efficacy of the BNT162b2 mRNA Covid-19 Vaccine', *https://doi.org/10.1056/NEJMoa2034577*, 383(27), pp. 2603–2615. Available at: https://doi.org/10.1056/NEJMOA2034577.

Pollara, J. *et al.* (2011) 'High throughput quantitative analysis of HIV-1 and SIV-specific ADCC-mediating antibody responses', *Cytometry. Part A : the journal of the International Society for Analytical Cytology*, 79(8), pp. 603–612. Available at: https://doi.org/10.1002/cyto.a.21084.

Rando, H.M. *et al.* (2021) 'Pathogenesis, Symptomatology, and Transmission of SARS-CoV-2 through Analysis of Viral Genomics and Structure', *mSystems*, 6(5). Available at: https://doi.org/10.1128/MSYSTEMS.00095-21/ASSET/6EDEDB25-0C63-49F2-A252-AAF523906B46/ASSETS/IMAGES/LARGE/MSYSTEMS.00095-21-F001.JPG.

Rastogi, M. *et al.* (2020) 'SARS coronavirus 2: from genome to infectome', *Respiratory Research 2020 21:1*, 21(1), pp. 1–15. Available at: https://doi.org/10.1186/S12931-020-01581-Z.

Rayati Damavandi, A. *et al.* (2022) 'Molecular variants of SARS-CoV-2: antigenic properties and current vaccine efficacy', *Medical Microbiology and Immunology*, 211(2–3), pp. 79–103. Available at: https://doi.org/10.1007/s00430-022-00729-6.

Richardson, S.I. *et al.* (2021) 'A SARS-CoV-2 variant of concern triggers Fc effector function with increased cross-reactivity', *medRxiv*, p. 2021.11.05.21265853. Available at: https://doi.org/10.1101/2021.11.05.21265853.

Richardson, S.I., Kgagudi, P., *et al.* (2022) 'Fc effector activity and neutralization against SARS-CoV-2 BA.4 is compromised in convalescent sera, regardless of the infecting variant'. bioRxiv, p. 2022.07.14.500042. Available at: https://doi.org/10.1101/2022.07.14.500042.

Richardson, S.I., Manamela, N.P., *et al.* (2022) 'SARS-CoV-2 Beta and Delta variants trigger Fc effector function with increased cross-reactivity', *Cell Reports Medicine*, 3(2). Available at: https://doi.org/10.1016/J.XCRM.2022.100510.

Richardson, S.I., Madzorera, V.S., *et al.* (2022) 'SARS-CoV-2 Omicron triggers cross-reactive neutralization and Fc effector functions in previously vaccinated, but not unvaccinated, individuals', *Cell Host & Microbe*, 30(6), pp. 880-886.e4. Available at: https://doi.org/10.1016/j.chom.2022.03.029.

Richardson, S.I. and Moore, P.L. (2021) 'Targeting Fc effector function in vaccine design', *Expert Opinion on Therapeutic Targets*, 25(6), pp. 467–477. Available at: https://doi.org/10.1080/14728222.2021.1907343.

Rogers, T.F. *et al.* (2020) 'Isolation of potent SARS-CoV-2 neutralizing antibodies and protection from disease in a small animal model', *Science (New York, N.Y.)*, 369(6506), pp. 956–963. Available at: https://doi.org/10.1126/SCIENCE.ABC7520.

Rössler, A. *et al.* (2022) 'SARS-CoV-2 Omicron Variant Neutralization in Serum from Vaccinated and Convalescent Persons', *New England Journal of Medicine*, 386(7), pp. 698–700. Available at: https://doi.org/10.1056/NEJMc2119236.

Sadoff, J. *et al.* (2022) 'Final Analysis of Efficacy and Safety of Single-Dose Ad26.COV2.S', *New England Journal of Medicine*, 386(9), pp. 847–860. Available at: https://doi.org/10.1056/NEJMOA2117608.

Schäfer, A. *et al.* (2021) 'Antibody potency, effector function, and combinations in protection and therapy for SARS-CoV-2 infection in vivo', *The Journal of Experimental Medicine*, 218(3). Available at: https://doi.org/10.1084/JEM.20201993.

Scheaffer, S.M. *et al.* (2023) 'Bivalent SARS-CoV-2 mRNA vaccines increase breadth of neutralization and protect against the BA.5 Omicron variant in mice', *Nature Medicine*, 29(1), pp. 247–257. Available at: https://doi.org/10.1038/s41591-022-02092-8.

Seow, J. *et al.* (2020) 'Longitudinal observation and decline of neutralizing antibody responses in the three months following SARS-CoV-2 infection in humans', *Nature Microbiology*. Available at: https://doi.org/10.1038/s41564-020-00813-8.

Shi, R. *et al.* (2020) 'A human neutralizing antibody targets the receptor-binding site of SARS-CoV-2', *Nature*, 584(7819), pp. 120–124. Available at: https://doi.org/10.1038/s41586-020-2381-y.

South Africa: WHO Coronavirus Disease (COVID-19) Dashboard With Vaccination Data (2023). Available at: https://covid19.who.int (Accessed: 26 February 2023).

Srinivasan, S. *et al.* (2020) 'Structural Genomics of SARS-CoV-2 Indicates Evolutionary Conserved Functional Regions of Viral Proteins', *Viruses*, 12(4). Available at: https://doi.org/10.3390/V12040360.

Starr, T.N. *et al.* (2021) 'Antibodies to the SARS-CoV-2 receptor-binding domain that maximize breadth and resistance to viral escape.', *bioRxiv* . Available at: https://doi.org/10.1101/2021.04.06.438709.

van der Straten, K. *et al.* (2022) 'Antigenic cartography using sera from sequence-confirmed SARS-CoV-2 variants of concern infections reveals antigenic divergence of Omicron', *Immunity*, 55(9), pp. 1725-1731.e4. Available at: https://doi.org/10.1016/J.IMMUNI.2022.07.018.

Tada, T. *et al.* (2021) 'Neutralization of Mu and C.1.2 SARS-CoV-2 Variants by Vaccine-elicited Antibodies in Individuals With and Without Previous History of Infection', *bioRxiv*, p. 2021.10.19.463727. Available at: https://doi.org/10.1101/2021.10.19.463727.

Tada, T. *et al.* (2022) 'High-titer neutralization of Mu and C.1.2 SARS-CoV-2 variants by vaccine-elicited antibodies of previously infected individuals', *Cell Reports*, 38(2). Available at: https://doi.org/10.1016/J.CELREP.2021.110237.

Tai, W. *et al.* (2022) 'Development of a ferritin-based nanoparticle vaccine against the SARS-CoV-2 Omicron variant', *Signal Transduction and Targeted Therapy*, 7(1), pp. 1–3. Available at: https://doi.org/10.1038/s41392-022-01041-8.

Tauzin, A. *et al.* (2021) 'A single dose of the SARS-CoV-2 vaccine BNT162b2 elicits Fc-mediated antibody effector functions and T cell responses', *Cell Host & Microbe*, 29(7), pp. 1137-1150.e6. Available at: https://doi.org/10.1016/J.CHOM.2021.06.001.

Terreri, S. *et al.* (2022) 'Persistent B cell memory after SARS-CoV-2 vaccination is functional during breakthrough infections', *Cell Host and Microbe*, 30, pp. 400-408.e4. Available at: https://doi.org/10.1016/j.chom.2022.01.003.

Tso, F.Y. *et al.* (2021) 'Presence of antibody-dependent cellular cytotoxicity (ADCC) against SARS-CoV-2 in COVID-19 plasma', *PLoS ONE*, 16(3 March). Available at: https://doi.org/10.1371/journal.pone.0247640.

Uriu, K. *et al.* (2021) 'Neutralization of the SARS-CoV-2 Mu Variant by Convalescent and Vaccine Serum', *New England Journal of Medicine*, 385(25), pp. 2397–2399. Available at: https://doi.org/10.1056/NEJMC2114706/SUPPL_FILE/NEJMC2114706_DISCLOSURES.PDF.

Uriu, K. *et al.* (2022) 'Characterization of the Immune Resistance of Severe Acute Respiratory Syndrome Coronavirus 2 Mu Variant and the Robust Immunity Induced by Mu Infection', *The Journal of Infectious Diseases*, 226(7), pp. 1200–1203. Available at: https://doi.org/10.1093/infdis/jiac053.

Viana, R. *et al.* (2022) 'Rapid epidemic expansion of the SARS-CoV-2 Omicron variant in southern Africa', *Nature*, 603(7902), pp. 679–686. Available at: https://doi.org/10.1038/s41586-022-04411-y.

Voysey, M. *et al.* (2021) 'Safety and efficacy of the ChAdOx1 nCoV-19 vaccine (AZD1222) against SARS-CoV-2: an interim analysis of four randomised controlled trials in Brazil, South

Africa, and the UK', *The Lancet*, 397(10269), pp. 99–111. Available at: https://doi.org/10.1016/S0140-6736(20)32661-1.

Walls, A.C. *et al.* (2020) 'Structure, Function, and Antigenicity of the SARS-CoV-2 Spike Glycoprotein', *Cell*, 181(2), pp. 281-292.e6. Available at: https://doi.org/10.1016/j.cell.2020.02.058.

Wang, P. *et al.* (2021) 'Antibody resistance of SARS-CoV-2 variants B.1.351 and B.1.1.7', *Nature 2021 593:7857*, 593(7857), pp. 130–135. Available at: https://doi.org/10.1038/s41586-021-03398-2.

Wang, Q. *et al.* (2022) 'Antigenic characterization of the SARS-CoV-2 Omicron subvariant BA.2.75', *Cell Host & Microbe*. Available at: https://doi.org/10.1016/J.CHOM.2022.09.002.

Weinreich, D.M. *et al.* (2021) 'REGN-COV2, a Neutralizing Antibody Cocktail, in Outpatients with Covid-19', *The New England Journal of Medicine*, 384(3), pp. 238–251. Available at: https://doi.org/10.1056/NEJMoa2035002.

Wibmer, C.K. *et al.* (2013) 'Viral Escape from HIV-1 Neutralizing Antibodies Drives Increased Plasma Neutralization Breadth through Sequential Recognition of Multiple Epitopes and Immunotypes', *PLOS Pathogens*, 9(10), p. e1003738. Available at: https://doi.org/10.1371/journal.ppat.1003738.

Wibmer, C.K. *et al.* (2021) 'SARS-CoV-2 501Y.V2 escapes neutralization by South African COVID-19 donor plasma', *Nature Medicine 2021 27:4*, 27(4), pp. 622–625. Available at: https://doi.org/10.1038/s41591-021-01285-x.

von Wintersdorff, C.J.H. *et al.* (2022) 'Infections with the SARS-CoV-2 Delta variant exhibit fourfold increased viral loads in the upper airways compared to Alpha or non-variants of concern', *Scientific Reports*, 12(1), p. 13922. Available at: https://doi.org/10.1038/s41598-022-18279-5.

Xia, S. *et al.* (2020) 'Fusion mechanism of 2019-nCoV and fusion inhibitors targeting HR1 domain in spike protein', *Cellular & Molecular Immunology 2020 17:7*, 17(7), pp. 765–767. Available at: https://doi.org/10.1038/s41423-020-0374-2.

Xiaojie, S. *et al.* (2021) 'Neutralizing antibodies targeting SARS-CoV-2 spike protein', *Stem Cell Research*, 50, p. 102125. Available at: https://doi.org/10.1016/J.SCR.2020.102125.

Yan, R. *et al.* (2020) 'Structural basis for the recognition of SARS-CoV-2 by full-length human ACE2', *Science*, 367(6485), pp. 1444–1448. Available at: https://doi.org/10.1126/SCIENCE.ABB2762.

Yang, L. *et al.* (2020) 'COVID-19 antibody therapeutics tracker: a global online database of antibody therapeutics for the prevention and treatment of COVID-19', *Antibody Therapeutics*, 3(3), pp. 205–212. Available at: https://doi.org/10.1093/abt/tbaa020.

Yang, Y. *et al.* (2022) 'Longitudinal analysis of antibody dynamics in COVID-19 convalescents reveals neutralizing responses up to 16 months after infection', *Nature Microbiology 2022*, pp. 1–11. Available at: https://doi.org/10.1038/s41564-021-01051-2.

Ye, Z.W. *et al.* (2020) 'Zoonotic origins of human coronaviruses', *International Journal of Biological Sciences*, 16(10), p. 1686. Available at: https://doi.org/10.7150/IJBS.45472.

Yu, F. *et al.* (2020) 'Receptor-binding domain-specific human neutralizing monoclonal antibodies against SARS-CoV and SARS-CoV-2', *Signal Transduction and Targeted Therapy*, 5(1). Available at: https://doi.org/10.1038/S41392-020-00318-0.

Zhao, Q. and He, Y. (2020) 'Challenges of Convalescent Plasma Therapy on COVID-19', *Journal of Clinical Virology*, 127, p. 104358. Available at: https://doi.org/10.1016/J.JCV.2020.104358.

Zhou, H. *et al.* (2019) 'Structural definition of a neutralization epitope on the N-terminal domain of MERS-CoV spike glycoprotein', *Nature Communications 2019 10:1*, 10(1), pp. 1–13. Available at: https://doi.org/10.1038/s41467-019-10897-4.

Zhou, P. *et al.* (2022) 'Broadly neutralizing anti-S2 antibodies protect against all three human betacoronaviruses that cause severe disease', *bioRxiv*n. Available at: https://doi.org/10.1101/2022.03.04.479488.

Zohar, T. and Alter, G. (2020) 'Dissecting antibody-mediated protection against SARS-CoV-2', *Nature Reviews Immunology*, 20(7), pp. 392–394. Available at:

https://doi.org/10.1038/s41577-020-0359-5.

7. Appendices

Appendix A: Supplementary figures

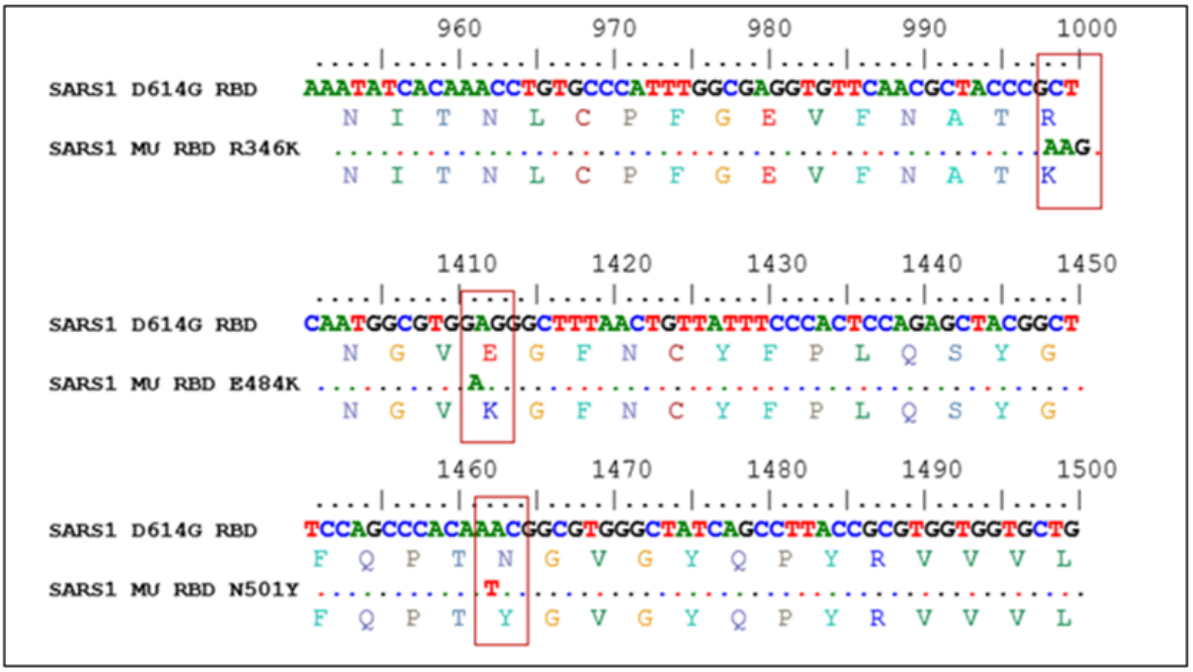

Figure A: Alignment of SARS-CoV-2 Mu RBD mutations to SARS-CoV-1 D614G chimera. Amino acid substitutions making up the mu RBD mutations are boxed in red.

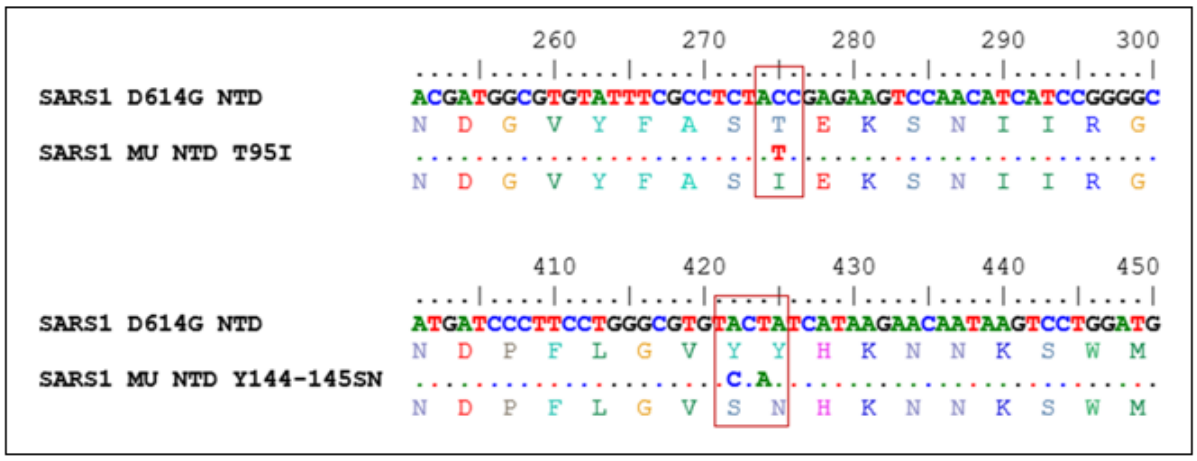

Figure B: Alignment of SARS-CoV-2 Mu NTD mutations to SARS-CoV-1 D614G chimera. Amino acid substitutions making up the Mu NTD mutations are boxed in red.

Appendix B: Ethics Clearance Certificate

UNIVERSITY OF THE WITWATERSRAND, JOHANNESBURG

R14/49 Prudence Kgagudi

HUMAN RESEARCH ETHICS COMMITTEE (MEDICAL)

CLEARANCE CERTIFICATE NO. M211142

NAME: (Principal Investigator)	Prudence Kgagudi
DEPARTMENT:	Virology National Institute for Communicable Diseases (NICD)
PROJECT TITLE:	Delineating sensitivity of globally emerging SARS-COV-2 variants to convalescent plasma from SARS-COV-2 infected donors
DATE CONSIDERED:	26/11/2021
DECISION:	Approved unconditionally
CONDITIONS:	
NOTE:	If contact information regarding student study participants is required, please contact the University Registrar's office <Nicoleen.Potgieter@wits.ac.za>
SUPERVISOR:	Prof P Moore
APPROVED BY:	Dr CB Penny, Chairperson, HREC (Medical)
DATE OF APPROVAL:	13/04/2022

This clearance certificate is valid for 5 years from date of approval. Extension may be applied for.

DECLARATION OF INVESTIGATORS

To be completed in duplicate and **ONE COPY** returned to the Research Office Secretary on the Third Floor, Faculty of Health Sciences, Phillip Tobias Building, 29 Princess of Wales Terrace, Parktown, 2193, University of the Witwatersrand. I/we fully understand the conditions under which I am/we are authorized to carry out the above-mentioned research and I/we undertake to ensure compliance with these conditions.Should any departure be contemplated, from the research protocol as approved, I/we undertake to resubmit the application to the Committee. **I agree to submit a yearly progress report.** The date for annual re-certification will be one year after the date of convened meeting where the study was initially reviewed. In this case, the study was initially reviewed in **November** and will therefore be due in the month of **November** each year. Unreported changes to the application may invalidate the clearance given by the HREC (Medical).

Principal Investigator Signature

22 APRIL 2022
Date

PLEASE QUOTE THE PROTOCOL NUMBER IN ALL ENQUIRIES